Noise Statistics in Optically Pre-Amplified DPSK Receivers with Optical Mach-Zehnder Interferometer Demodulation

Zhenqian Qu

A Thesis

in

The Department

of

Electrical and Computer Engineering

Presented in Partial Fulfillment of the Requirements

for the Degree of Master of Applied Science at

Concordia University

Montreal, Quebec, Canada

May 2004

Your file Votre référence
ISBN: 0-612-94708-4
Our file Notre référence
ISBN: 0-612-94708-4

Abstract

Noise Statistics in Optically Pre-Amplified DPSK Receivers with Optical Mach-Zehnder Interferometer Demodulation

Zhenqian Qu

A comprehensive theoretical analysis of noise statistics in optically pre-amplified DPSK receivers with optical Mach-Zehnder interferometer demodulation is presented for the first time. For such a receiver, there are three dominant noise sources which degrade the performance of DPSK systems: signal-ASE beat noise, ASE-ASE beat noise, and nonlinear phase noise. The first two noise sources are added to the signal, and thus they can be referred to as linearly additive noise. The detailed derivations of the exact noise statistics considering both the linearly additive noise and nonlinear phase noise are given in this thesis. Due to simplicity, the Gaussian approximation has been widely used in the case of optical systems with intensity modulation and direct detection (IM/DD). Therefore, the Gaussian approximation of noise statistics is also given and compared with the exact noise statistics in DPSK receivers. Numerical calculations show that the exact noise statistics are quite different from the Gaussian approximation, particularly for DPSK receivers with balanced detection. The numerical results of probability density functions and bit error rate with the exact noise statistics are in good agreement with the published experimental results. A comparative study of noise statistics in both DPSK and IM/DD receivers is also given.

Acknowledgments

I would like to take this opportunity to sincerely thank my supervisor, Dr. John X. Zhang, for providing me with this research topic and the useful guidance.

Finally, I would like to express my deepest and most sincere gratitude to my parents, and my sisters who have always been there for me.

Contents

List of Figures

Chapter 1

Introduction

1.1 The Evolution of Optical Fiber Communications Systems

Although optical communication, for instance by fires, smoke and optical telegraphs, has been used since a long time ago for information transmission, the research of optical fiber communication started around 1975. It has gained dramatic improvement during the past three decades.

In the U.S., the first commercial system at 0.85 um was deployed in the Chicago area during 1978. This system operated at a bit rate of 45 Mbps and achieved a repeater spacing of about 10 km. Meanwhile, in England, Standard Telecommunications Laboratories carried out a field trial at 144 Mbps over a span of 9 km [1]. These systems utilized GaAs/AlGaAs semiconductor lasers/LEDs, multimode fibers, and direct detection receivers.

The systems operating wavelength of 1.3 um became available in the early 1980s, but the bit rate was limited to below 100 Mb/s because of dispersion in multimode fibers. The limitation was overcome by the use of single-mode fibers. By 1987, they operated at bit rates of up 1.7 Gb/s with a repeater spacing of about 50 km [2]. The practical implementation of these devices marked the beginning of the second generation of

lightwave systems.

The third generation systems operated near 1.55 um and the signal is regenerated periodically by using electronic repeaters spaced apart typically by 60-70 km. The repeater spacing can be increased by making use of a homodyne or heterodyne detection scheme because its use improves receiver sensitivity. Such systems are referred to as coherent lightwave systems [2]. Systems operating at 1.55 um provide the lowest attenuation, but standard silica fibers have much larger signal dispersion at 1.55 um than at 1.3 um. Fiber manufacturers overcame this limitation by creating the so-called dispersion shifted fibers [3].

The fourth generation of lightwave systems makes use of optical amplification for increasing the repeater spacing and wavelength-division multiplexing (WDM) for increasing the bit rate. The introduction of optical amplifiers gave a major boost to fiber transmission capacity. In 1990, Bell Labs transmitted a 2.5 Gb/s signal over 7,500 km without regeneration. The system used a soliton laser and an erbium-doped fiber amplifier (EDFA) that allowed the light wave to maintain its shape and density. By 1996, not only transmission over 11,300 km at a bit rate of 5 Gb/s had been demonstrated by using actual submarine cables, but also commercial transatlantic and transpacific cable systems became available [2, 4]. Since then, a large number of submarine lightwave systems have been deployed worldwide.

The fifth generation of fiber-optic communication systems is concerned with extending the wavelength range over which a WDM system can operate simultaneously. The conventional wavelength window, known as the C band, covers the wavelength range 1.53-1.57 um. It is being extended on both the long- and short- wavelength sides.

resulting in the L and S bands, respectively. Fig. 1.1 shows the applications of optical fiber communication systems in the electromagnetic spectrum. The Raman amplification technique can be used for signals in all three wavelength-bands. The fifth-generation systems also attempt to increase the bit rate of each channel within the WDM signal. Because of fiber optic technology's immense potential bandwidth, 50 THz or greater, there are extraordinary possibilities for future fiber optic applications [2, 4]. Optical fiber communication has been developed so rapidly during the last 30 years that it has become the backbone of our communications systems.

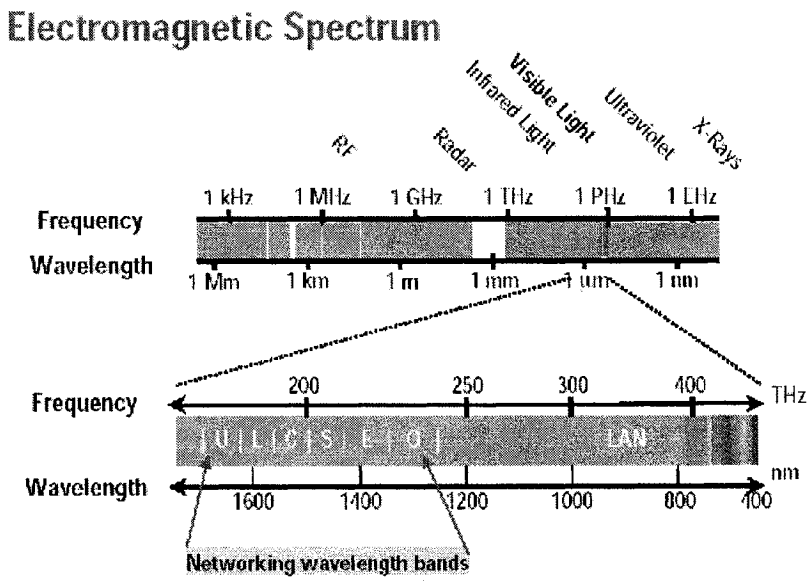

Fig. 1.1 Applications of optical fiber communication systems in the electromagnetic spectrum.

1.2 System Applications

Higher and higher capacities of transmitting enormous amounts of information across large distances were demanded in telecommunications networks. The technologies that were used extensively before, such as coaxial cable, satellite and microwave radio for

transferring information could not satisfy the growing requirement. With the introduction of fiber optic communications systems, the solution to the problems of transmission capacity shortage has been successfully found [5]. Compared to copper cable transmission and radio and microwave transmission, optical fiber transmission systems are far easier to design and understand. Optical fibers, due to not only, their beneficial characteristic for information transmission as low attenuation and dispersion, large bandwidth, immunity to electrical noise, but also for their durability, and flexibility, became soon part of telecommunication network infrastructure [6].

Now the optical fiber communication system encompasses the transmission of voice, video, and data signals to a variety of applications due to many advantages. The voice transmission includes telephone trunk, interoffice, intercity, subscriber loops, and transoceanic applications. Video is used for television industry, remote monitoring, and surveillance applications. The broadcast television industry uses lightwave transmission for short distances such as studio to the transmitter or live event to the equipment van. The cable television industry picks up signals from several sources, including antennas, satellite, and microwave links. All the signals from these sources are transmitted simultaneously along a single fiber. The data applications include computer networks such as interoffice data links, local-area networks (LANs), metropolitan-area networks (MANs), and wide-area networks (WANs). The interoffice data links include the connection of different computers with different buildings within a university campus or a city. The LAN connects various computers within a building or a region. The MAN is used to link computers within the metropolitan area, and the WAN is used for linking various cities in the same region [1]. Until now the optical fiber communication systems

have been employed in many areas of telecommunication.

1.3 Optical Modulation Formats

The optical system can utilize the amplitude-, frequency-, and phase-shift keying modulation formats. Each format has certain advantages and disadvantages from an overall system viewpoint. Fig. 1.2 shows schematically these modulation formats.

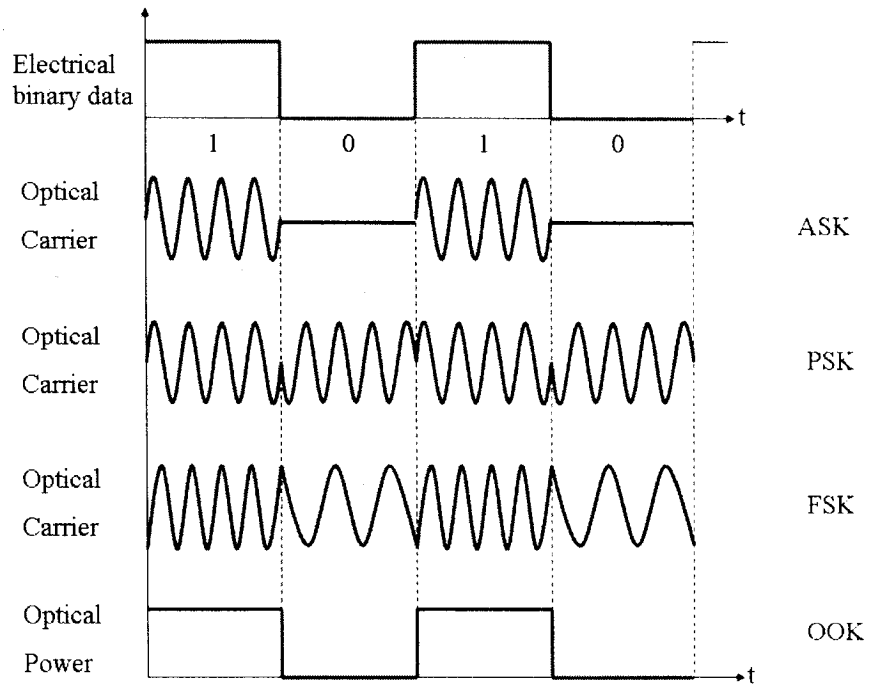

Fig.1.2 ASK, PSK, FSK, and OOK modulation formats

Amplitude Shift Keying (ASK) is an extremely simple modulation format to generate. The electric field associated with an optical signal can be written as

$$E_s(t) = A_s(t)\cos[\omega_0 t + \phi_s(t)] \tag{1.1}$$

In the case of ASK format, the amplitude A_s is modulated while keeping ω_0 and ϕ_s constant. For binary digital modulation, A_s take one of the two fixed values during

each bit period, depending on whether bit "1" or "0" is being transmitted. In most practical situations, A_s is set to zero during transmission of "0" bit. The implementation of ASK for coherent systems differs from the case of the direct-detection systems in one important aspect. External modulation is necessary for coherent communication systems. The reason behind this necessity is related to phase changes that invariably occur when the amplitude is changed by modulating the current applied to a semiconductor laser [2]. The detector response of coherent systems depends on the phase of the received signal. The implementation of ASK format for coherent systems requires the phase to remain nearly constant. This is achieved by using an external modulator.

A modulation scheme that is popular because of its simplicity is on-off keying (OOK) illustrated in Fig. 1.2. The laser output is simply turned on and off in response to whether the data is "1" or "0". This format is particularly popular with noncoherent IM/DD digital lightwave systems. For nonreturn-to-zero signals, the laser is turned on when transmitting a "1" and stays on for the entire bit time. A variation on OOK is return-to-zero signaling, where the laser is on during a bit "1" but for a time that is less than the bit time. This format is commonly found in short-pulse and soliton systems [7].

In Frequency-Shift-Keying (FSK) systems, the transmitter generates a specific frequency for bit "1" and a different frequency for bit "0". In Phase-Shift-Keying (PSK) and Differential-Phase-Shift-Keying (DPSK) systems, the transmitted signal's envelope is held constant while a phase transition is sent to indicate digital information such as 0 is for bit "0" and π is for bit "1". In Eq. (1.1), the optical bit is generated by modulating the phase ϕ_s, whereas the amplitude A_s and the frequency ω_0 of the optical carrier are kept constant.

1.4 Detection Schemes

1.4.1 Direct Detection

The simplest form of a classical direct detection communications receiver is one that performs simple energy detection. If the receiver detects light of sufficient intensity it outputs a logical *one*; otherwise the receiver output is a logical *zero*. Direct detection receivers are typically thought of as being able to respond only to intensity fluctuations in the received optical signal. Phase, frequency, and polarization information is often not considered in a direct detection communication system.

One standard modulation/demodulation scheme being employed in the present optical fiber communications is called the intensity-modulation/direct-detection (IM/DD) scheme in which an electrical bit stream modulates the intensity of an optical carrier inside the optical transmitter and the optical signal transmitted through the fiber link is incident directly on an optical receiver, which converts it to the original digital signal in the electrical domain. The IM stems from two facts. One is the light intensity (not the amplitude) is modulated linearly with respect to the signal voltage and another one is that no attention is paid to the phase of the carrier. The term DD stems from that the signal is detected directly at the optical stage of the receiver [2, 8]. The function of an optical receiver is to detect and extract the information signal from the modulated optical wave. The information may be analog or digital, which is modulated by intensity modulation (IM) or external modulation schemes. The photodetectors such as an APD or a PIN diode are used for converting the incident modulated optical wave into an electrical signal. Then the electrical signal is amplified and filtered, and the output signal is sent to the decision circuit.

By utilizing additional optical elements for FSK and DPSK, it is possible to construct direct-detection receivers. For a FSK signal, an optical frequency discriminator such as a Fabry-Perot can be used before direct detection. For DPSK, an optical Mach-Zehnder interferometer (MZI) can be used in front of the photodetector [7]. In DPSK system, the Mach-Zehnder interferometer converts the phase information into intensity information.

1.4.2 Coherent Detection

Some communication systems transmit information by modulating the frequency or the phase of the optical carrier and detect the transmitted signal by using homodyne or heterodyne detection techniques. Since a local optical carrier is used in the implementation of such receivers, such optical communication systems are called coherent lightwave systems. Coherent transmission techniques were studied during 1980s. Fig 1.3 shows the basic principle of operation involved in a coherent system.

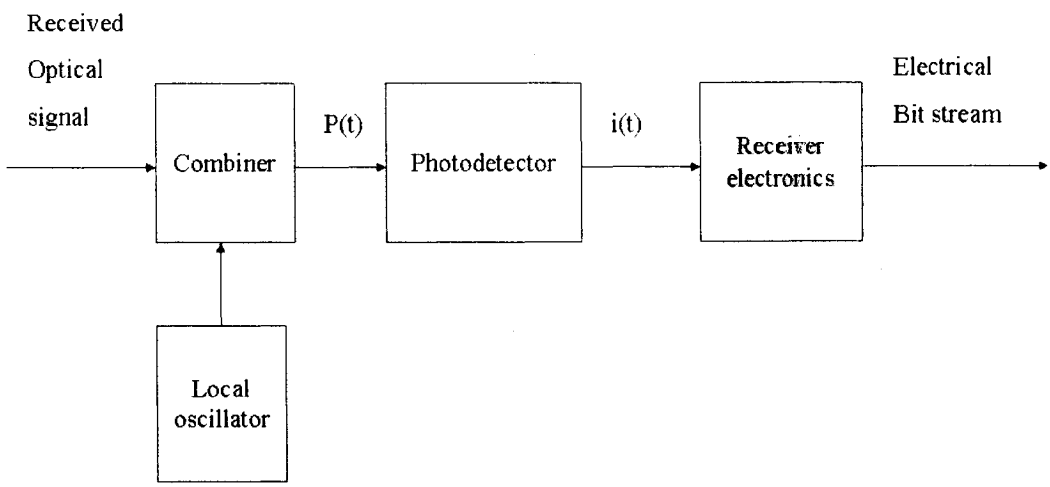

Fig. 1.3 Basic principle of a coherent receiver

The basic idea behind coherent detection consists of combining the optical signal coherently with a continuous-wave (CW) optical field before it enters into the photodetector. The CW field is generated locally at the receiver using a narrow linewidth laser, called the local oscillator (LO) [2]. In fact, there are two different coherent detection techniques to choose, depending on whether or not the local-oscillator frequency ω_{LO} equals signal-carrier frequency ω_0. They are known as homodyne and heterodyne detection techniques.

1.5 Motivation for Research

Binary OOK has been widely used in wavelength division multiplexing (WDM) communication systems because of simplicity. In such a system, there are some performance penalties induced by chromatic dispersion, self-phase modulation (SPM), cross-phase modulation (XPM), four wave mixing (FWM), and amplified spontaneous emission (ASE) noise etc.. As the channel spacing of dense WDM (DWDM) transmission is decreased, the XPM induced by Kerr effect between channels becomes one of major limitations. One solution of reducing the XPM effect is to use phase modulation. Therefore, DPSK combined with Mach-Zehnder interferometer (MZI) demodulation has been attracted a great attention such as a breakthrough experiment, transmitting 1.6 Tb/s (40 channels at 40 Gb/s) over 10,000 km [9, 10]. Later it was found that the receiver sensitivity by DPSK receivers with balanced detection is 3 dB better than that in IM/DD receivers [11-22]. Thus, the advantages of using DPSK modulation format are two folds: one is to reduce XPM-induced penalties in DWDM transmission systems, and the other one is 3 dB improvement in receiver sensitivity by DPSK receivers over IM/DD receivers

if the balanced detection is employed in DPSK receiver. This 3 dB advantage gives an increased system margin, which can be used to reduce the input power to the fiber spans or to increase the length of the fiber link. In a system limited by ASE induced beat noise, a 3 dB receiver sensitivity gain directly translates into twice the transmission distance. In order to analyze transmission performance, noise statistics of the DPSK receivers have to be investigated. To the best of our knowledge, a comprehensive theoretical analysis of noise statistics in DPSK receivers has not been given so far.

In optically pre-amplified DPSK and IM/DD receivers, there are mainly two noise sources: signal-ASE beat noise and ASE-ASE beat noise. All other noise contributions can be ignored such as thermal noise and shot noise since their impact is very small and negligible. The signal-ASE beat noise has the Gaussian noise statistic and it is usually dominant. Thus, Gaussian noise can be considered as a fair approximation of noise statistics which has been widely used in IM/DD receivers. On the other hand, the exact noise statistic in IM/DD receivers has been analyzed [23, 24], and it is found the exact pdf is Chi-square distribution. However, the noise statistics in IM/DD receivers can not be directly applied for the case of DPSK receivers.

Besides, DPSK transmission can be degraded by phase noise. In WDM systems, there are three sources of phase noise: (1) laser phase noise, which is usually negligible in high bit rate transmission [11], (2) linear phase noise generated by the direct contribution of ASE noise, which is linearly increased as the number of optical amplifiers and is not particularly severe [25], (3) nonlinear phase noise induced by the interaction of *Kerr effect* and ASE noise, which is directly dependent on signal power along the fiber. Usually the nonlinear phase noise is dominant among them in the practical WDM

transmission systems. If the phase noise is included into the noise statistics, the pdf of noise statistics in DPSK/MZI receivers has not been given theoretically except the measurement [26].

1.6 Contributions and Scope of Thesis

The major contributions of the thesis are listed below:

1. A theoretical analysis on optically pre-amplified DPSK receivers with optical Mach-Zehnder interferometer demodulation is presented for the first time, in which both ASE noise and nonlinear phase noise are included.
2. Derivations of the exact analytical expressions and Gaussian approximations for probability density functions in DPSK systems are given. The numerical calculated results in exact noise statistics are in good agreement with the published experimental results.
3. A comparative study of noise statistics in both DPSK and IM/DD receivers is given.

Chapter 2 first gives the structure of the DPSK systems, and then the functions and fundamental knowledge of the components in the systems will be introduced. Chapter 3 presents some fundamental knowledge and statistical properties of noise sources such as linearly additive noise and nonlinear phase noise. In Chapter 4, the effects of linearly additive noise and nonlinear phase noise on the DPSK receivers are discussed. Derivations of exact analytical expressions and Gaussian approximations will been given. We compare the difference of the noise statistic for DPSK and IM/DD receivers. The

impact of optical and electrical filtering is also discussed in this Chapter. Chapter 5 summarizes the work in this thesis, and then suggestions about future work are given.

Chapter 2

DPSK System Structure and Components

2.1 System Structure

A DPSK system is configured schematically in Fig. 2.1. Each transmitted symbol conveys one bit, which is encoded in $\Delta\Phi$, the phase difference between successive symbols. An electronic pre-coder before optical modulator is needed to ensure that the phase shifts of the optical signal can be correctly decoded at the receiver. Since direct-detection receivers do not provide an absolute optical phase reference, the phase reference has to be provided by the signal itself, and information has to be encoded on the optical phase difference between bits. In this thesis, a logical "1" is represented by no phase shift and a logical "0" is represented by a π phase shift between two adjacent optical bits. Differential encoding can be done entirely in the digital domain using a one bit delay feedback and an exclusive or (XOR) gate [27].

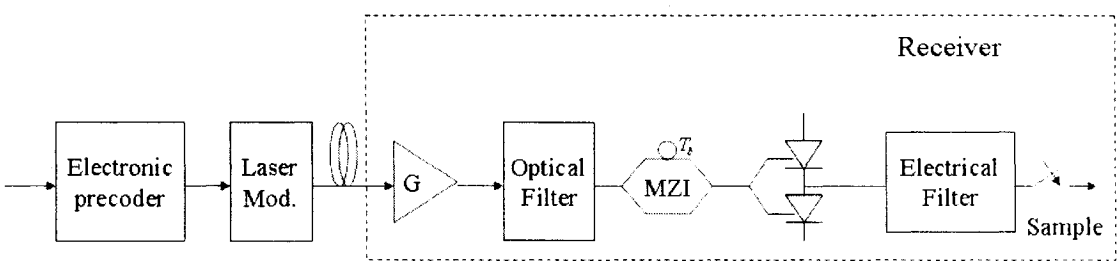

Fig. 2.1 Schematic structure of DPSK system with MZI demodulation

The optical source is assumed to be a single-frequency laser whose linewidth is negligible in comparison to the symbol rate, so that laser phase noise is negligible. External modulation is used to obtain the DPSK optical signal.

The received optical signal passes into an optical pre-amplifier, which adds amplified spontaneous emission (ASE) noise into the signal. The optical preamplifier in Fig. 2.1 is assumed to have flat gain G. We assumed the ASE noise as additive white Gaussian noise (AWGN) with power spectral density $n_{sp}(G-1)hv$ in each polarization, where $n_{sp} \geq 1$ is the spontaneous emission parameter and hv is the photon energy [3]. We assume that the gain G is sufficiently high that ASE dominates over shot noise and thermal noise in the receiver, allowing us to ignore the latter two noise contributions.

Because adding amplified spontaneous emission (ASE) will degrade the optical signal-to-noise ratio (OSNR) at the receiver, the amplifier output is filtered by an optical bandpass filter with bandwidth B_o to reduce ASE noise. In DPSK receivers, we use an optical Mach-Zehnder delay interferometer as a phase-to-intensity converter. The Mach-Zehnder delay interferometer (MZI) with a delay equals to the bit period T_b optically decodes the data and converts it into two intensity modulated signals, which are the sum and difference of the signals on the two arms of the MZI. The path differences within the delay interferometer are fine-tuned for destructive or constructive interference at output ports in the absence of phase modulation. A balanced optical detection yields a photocurrent proportional to the difference between the intensities at the two interferometer output ports. This photocurrent is lowpassly filtered by an electrical lowpass filter with bandwidth B_e. Finally, the electrically filtered signal is sampled, and electrical data is regenerated.

2.2 Transmitter

The role of the optical transmitter is to convert an electrical input signal into the corresponding optical signal and then the optical signal is launched into the optical fiber serving as a communication channel.

2.2.1 Optical Sources

The major component of optical transmitters is an optical source. Fiber-optic communication systems often use semiconductor optical sources such as light-emitting diodes (LEDs) and semiconductor lasers because of several inherent advantages offered by them. Some of these advantages are compact size, high efficiency, good reliability, right wavelength range, small emissive area compatible with fiber core dimensions, and possibility of direct modulation at relatively high frequencies. Although the operation of semiconductor lasers was demonstrated as early as 1962, their use became practical only after 1970, when semiconductor lasers operating continuously at room temperature became available [2]. Since then, semiconductor lasers have been developed extensively because of their importance for optical communications. There are two types of semiconductor lasers: multi-frequency lasers and single frequency lasers. The main difference between these lasers is their spectrum. The multi-frequency lasers oscillate in several longitudinal modes simultaneously due to the small gain (or loss) difference between the adjacent modes, which results in many frequency components. Conversely the single frequency laser oscillates in a single longitudinal mode (dominant mode) and whereas the other modes are discriminated by their higher loses, resulting in a single frequency component. The semiconductor lasers offer higher power output. higher

modulation bandwidth, and narrower spectral width than the LEDs. In contrast to lasers. LEDs make use of the incoherent light emission from the spontaneous emission of carriers. The LED device structure is compatible with multimode fibers and achieves higher light-coupling efficiency [1].

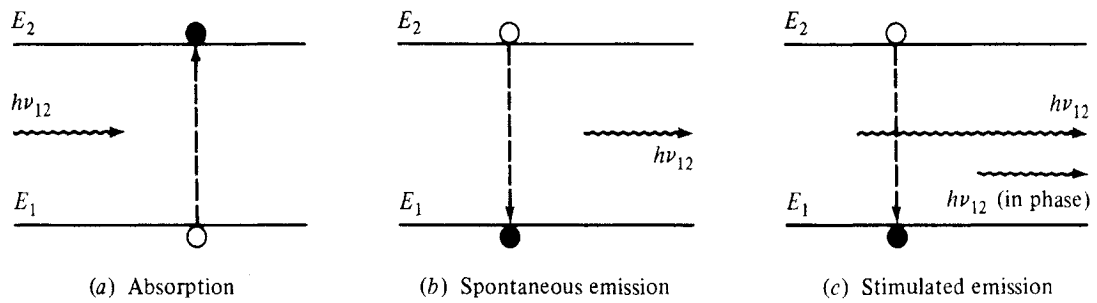

(*a*) Absorption (*b*) Spontaneous emission (*c*) Stimulated emission

Fig. 2.2 Three fundamental processes occurring between the two energy states of an atom

The fundamental theory for the design and construction of LED and laser optical sources is based on electron hole recombination within a semiconductor material. This electron hole recombination results in a generation of photons that have frequencies that are determined by the physical parameters of the semiconductor material. The two phenomena derived from the interaction between matters and light are emission and absorption. Emission can also be divided into two basic categories: *stimulation emissions* and *spontaneous emissions*, which are shown in Fig. 2.2. An electron of energy E_1 can be elevated to level E_2 by absorbing a photon of energy $E = hf$. An electron that is already at energy level E_2 can decay to energy level E_1 by releasing a photon (spontaneous emission). The third phenomenon is observed when an electron already at energy level E_2 absorbs a photon and decays to energy level E_1. Through this process,

two photons that have the exact same phase direction and energy levels are simultaneously released. If continuous radiation is maintained, the generation of photons will also be continued (stimulation emission). LED operation is based on spontaneous emission, while the laser operation is based on stimulated emission [28]. In general, for both devices, the principle of operation is based on the interaction of light and matter within a semiconductor material.

2.2.2 Direct and Indirect Modulation

In transmitter model, depending on whether the output light is modulated by directly modulating the current source to the laser or whether the light is modulated externally after it has been generated, the process of modulation can be classified as either direct or indirect (external) modulation. With direct modulation, the light is directly modulated inside the light source, while external modulation uses a separate external modulator placed after the laser source.

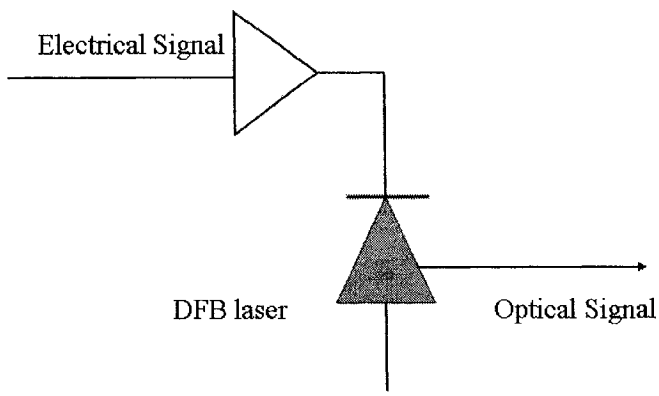

Fig.2.3 Direct modulation

Direct modulation is used in many optical communication systems owing to its simple and cost-effective implementation. However, due to the physics of laser action,

the light output under direct modulation can not respond to the input electrical signal instantaneously. Instead, there are delays and oscillations that occur when modulating the signal, which is used as the pumping current, has large and fast changes. As a result, direct modulation has several undesirable effects, such as frequency chirping and linewidth broadening [29].

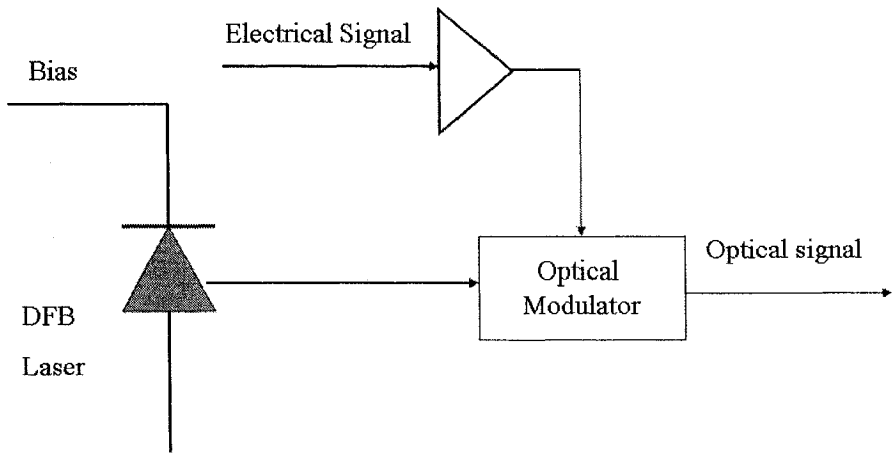

Fig.2.4 External modulation

External modulation provides an alternative approach to achieve light modulation with the added benefit of avoiding the undesirable frequency chirping effects in DFB lasers. A typical external modulator consists of an optical waveguide in which the incident light propagates through and the refractive index or absorption of the medium is modulated by a signal that represents the data to be transmitted. The typical desirable properties of an external modulator from a communication perspective are a large modulation bandwidth, a large depth of modulation, a small insertion loss of the signal light passing through the device, and a low electrical drive power [29].

2.3 Optical Fibers

A number of requirements must be fulfilled in selecting material for optical fiber fabrication. Material must obviously be a dielectric which is highly transparent over the wavelength range where the fiber is to be used. It must also be capable of being drawn into a fiber form and yet preserve its basic optical and mechanical properties. A good fiber material must also permit the possibility of smoothly varying its refractive index by the addition of dopants. *Glasses* and *plastics* are the two categories of materials that generally satisfy these requirements. Silicate glasses are the most widely used for fiber fabrication and the availability of ultra-pure and highly-transparent silicate glass fibers has made them the preferred choice for long-haul transmission in the near-infrared. Other glasses with good transmission potential exist, but the constraints imposed by fiber fabrication significantly limit their application. Recent advances in plastic fiber fabrication have also made them an excellent choice for short distance applications, where loss considerations are of lesser concern. Plastic fibers are the most economical solution to the transmission of visible light over relatively short distances. The use of plastic fibers in communication networks is of great interest for application where the transmission distances are between tens of centimeters and a few hundred meters [30].

2.3.1 Basic Optical Principals

In order to understand the functionality of optical fiber, we first study the basic concepts and definitions. A fundamental optical parameter of a material is the *refractive index*. In free space a light wave travels at a speed $c = 3 \times 10^8 m/s$. The speed of light is related to the frequency v and the wavelength λ by $c = v\lambda$. When entering a

dielectric or nonconducting medium the wave now travels at a speed υ, which is characteristic of the material and is less than c. The ratio of the speed of light in a vacuum to in matter is the index of refraction n of the material and is given by $n = c/\upsilon$. Typical values of n are 1.00 for air, 1.33 for water, 1.50 for glass, and 2.42 for diamond [3]. The concepts of *reflection* and *refraction* can be interpreted most easily by considering the behavior of light rays associated with plane waves traveling in a dielectric material. When a beam of light hits the interface between optical media, a part of the light will be reflected back into the first medium and the remainder is bent or refracted as it enters the second material.

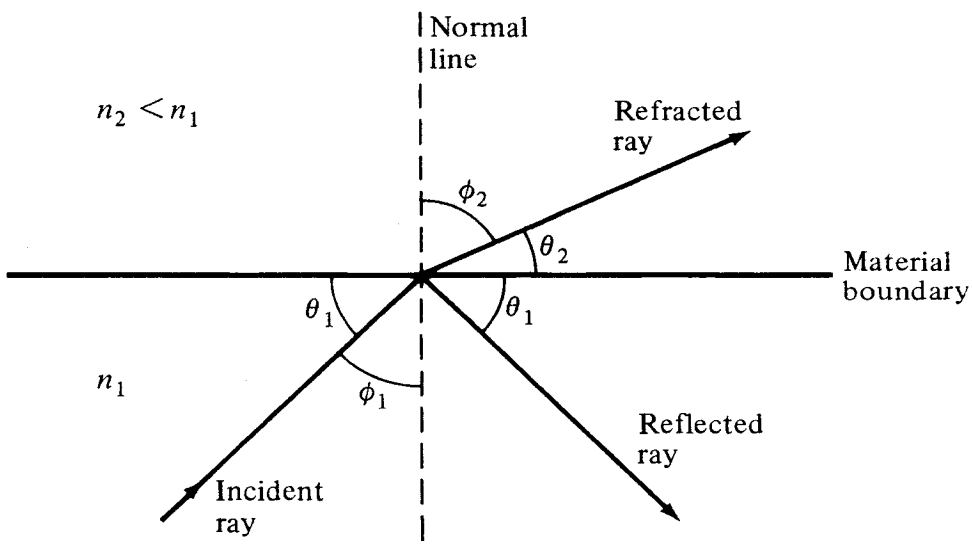

Fig. 2.5 Refraction and reflection of a light ray at a material boundary

In Fig. 2.5 [3], the bending or refraction of the light ray at the interface is a result of the difference in the speed of light in two materials that have different refractive indices. The relationship at the interface is known as Snell's law and is given by

$$n_1 \sin\phi_1 = n_2 \sin\phi_2 \tag{2.1}$$

2.3.2 Properties of Optical Fibers

Loss is an important characteristic of optical fibers. Signal attenuation in optical fibers arises from many sources, related either to the material or to the waveguide itself. Depending on the fiber material used, the relative weight of these various contributions will vary as a function of wavelength, leading to qualitatively different spectral characteristics. Fig. 2.6 shows the loss spectrum of optical fiber.

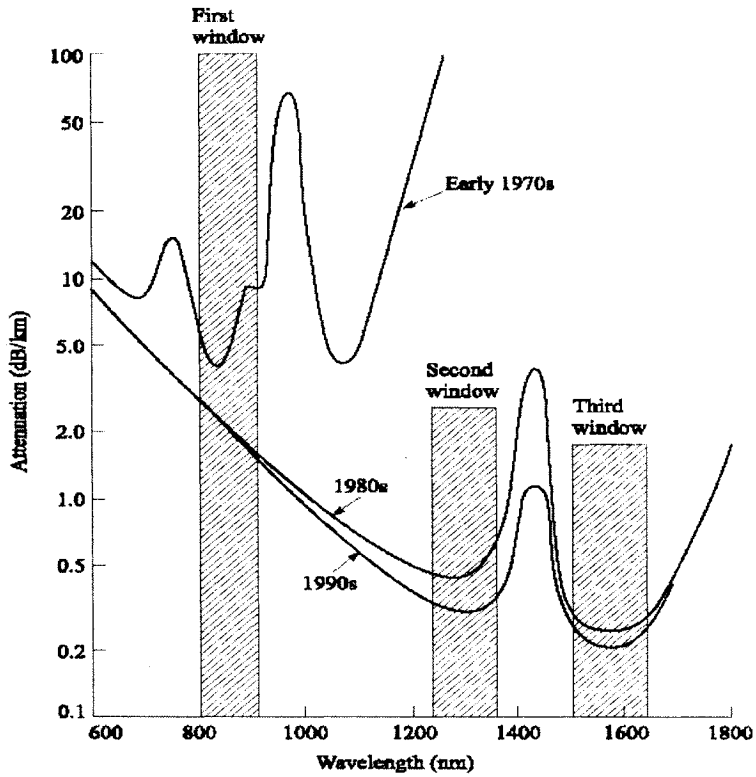

Fig. 2.6 Loss spectrum of optical fiber [3]

There are three major mechanisms that are responsible for losses: material absorption, *Rayleigh scatting*, and waveguide imperfections [2]. Light is absorbed by the material. Although the glass used for optical fibers has an extremely low absorption coefficient, a little light is still lost due to this effect. *Rayleigh scattering* is a fundamental loss

mechanism arising from local microscopic fluctuations in density. Silica molecules move randomly that leads to random fluctuations of the refractive index on a scale smaller than the optical wavelength λ. Light scattering in such a medium is known as *Rayleigh scattering*. An ideal single-mode fiber with a perfect cylindrical geometry guides the optical mode without energy leakage into the cladding layer. In practice, imperfections at the core-cladding interface can lead to additional losses which contribute to the net fiber loss.

Compared to loss, dispersion is an effect a bit harder to imagine. In fact, all the light waves do not travel at the same speed; and all colors have their particular velocities. In transmission technology, dispersion is the tendency for optical pulses to spread as they travel through the optical fiber. The reason is that each pulse consists of a variety of different wavelength, each traveling at its own speed. As a consequence it becomes more difficult to distinguish if a received bit is "1" or "0". This effect is called Inter-Symbol-Interference (ISI).

Electromagnetic waves are three dimensional waves. Optical waves are electromagnetic wave occupying a narrow band of the electromagnetic spectrum. Fig. 2.7 shows an electromagnetic wave in three dimensional planes. Usually such optical waves, generated by natural of man-made sources are referred to as *unpolarized waves*. However, in numerous applications, the electric field vector component of the optical ray must occupy only one plane. In order to achieve this, the three dimensional electromagnetic wave must be transformed to as *polarization*. Polarization of light is referred to as the process whereby the electric field vector component vibrates in a single plane, producing a sinewave laying on the plane of polarization [28].

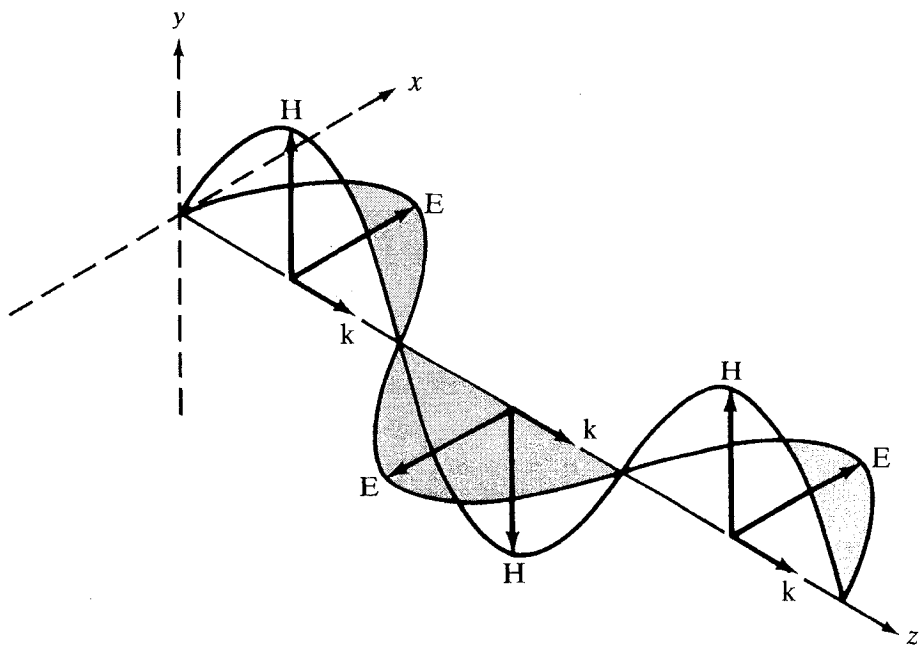

Fig. 2.7 An electromagnetic wave

2.4 Optical Amplifiers

The transmission distance of any fiber-optic communication system is eventually limited by fiber losses. For long-haul systems, the loss limitation has traditionally been overcome using optoelectronic repeaters in which the optical signal is first converted into an electric current and then regenerated using a transmitter. Such regenerators become quite complex and expensive for wavelength division multiplexed (WDM) lightwave systems. An alternative approach to loss management makes use of optical amplifiers, which amplify the optical signal directly without requiring its conversion to the electric domain. Several kinds of optical amplifiers were developed during the 1980s, and the use of optical amplifiers for long-haul lightwave systems became widespread during the 1990s [2]. Fig.2.8 shows a general optical amplifier structure.

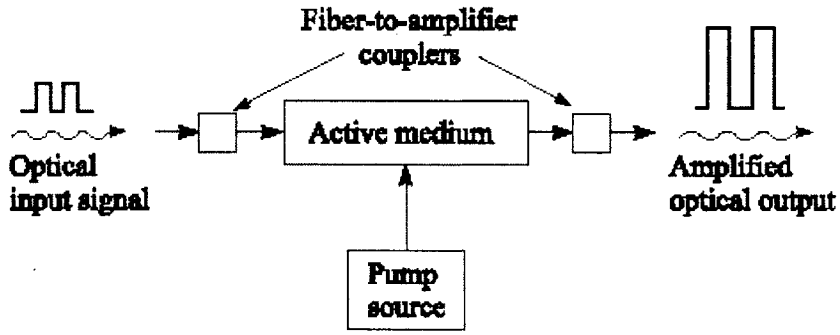

Fig.2.8 A general optical amplifier structure

2.4.1 Applications of Optical Amplifiers

Optical amplifiers can serve several purposes in the design of fiber-optic communication systems: three common applications are shown schematically in Fig. 2.9, which are in-line amplifier, booster amplifier, and pre-amplifier.

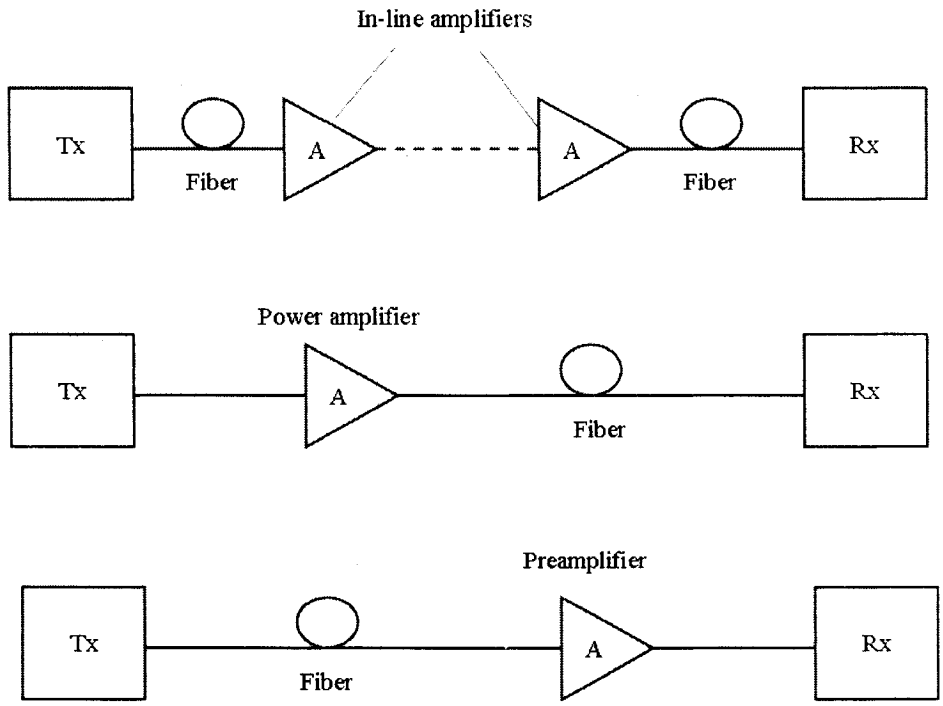

Fig. 2.9 Three applications of optical amplifiers

The most important application for long-haul systems consists of using amplifiers as in-line amplifiers which replace electronic regenerators. Many optical amplifiers can be cascaded in the form of a periodic chain as long as the system performance is not limited by the cumulative effects of fiber dispersion, fiber nonlinearity, and amplifier noise. Another way to use optical amplifiers is to increase the transmitter power by placing an amplifier just after the transmitter. Such amplifiers are called power amplifier or power boosters, as their main purpose is to boost the power transmitted. A power amplifier can increase the transmission distance by 100km or more depending on the amplifier gain and fiber losses. Transmission distance can also be increased by putting an amplifier just before the receiver to boost the received power. Such amplifiers are called optical preamplifiers and are commonly used to improve the receiver sensitivity [2].

2.4.2 Erbium-Doped Fiber Amplifiers

An important class of fiber amplifiers makes use of rare-earth elements as a gain medium by doping the fiber core during the manufacturing process. Amplifier properties such as the operating wavelength and the gain bandwidth are determined by the dopants rather than by silica fiber, which plays the role of a host medium. Many different rare-earth elements, such as erbium, holmium, neodymium, samarium, thulium, and ytterbium, can be used to realize fiber amplifiers operating at different wavelengths in the range 0.5-3.5 um. Erbium-doped fiber amplifiers (EDFAs) have attracted the most attention because they operate in the wavelength region near 1.55um [2]. The basic EDFA configuration is shown in Fig. 2.10.

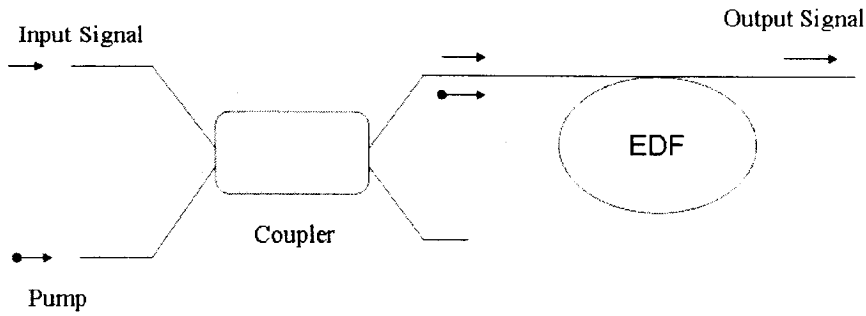

Fig. 2.10 Basic EDFA configuration

The diode pump output and the incoming signal are combined through a coupler and are launched into a short length of optical fiber containing a low concentration of erbium ions. Pump photons excite the rare-earth ions which, in turn, give efficient signal amplification in the 1.55 um wavelength region, provided that adequate population inversion is achieved. EDFAs are shown to provide extremely high gain, low noise figure and high saturation output powers over a wide bandwidth. These general characteristics render EDFAs ideal for use as boosters, in-line amplifiers and preamplifiers [30].

2.4.3 Amplifier Gain and Noise Figure

One of the most important parameters of an optical amplifier is the signal gain or amplifier gain G is defined as

$$G = \frac{P_{s,out}}{P_{s,in}} \tag{2.2}$$

where $P_{s,in}$ and $P_{s,out}$ are the input and output powers, respectively, of the optical signal being amplified. Fig.2.11 illustrates the dependence of the gain on the input power. The curve shows that as the input signal power is increase, the gain first stays near the

small-signal level and then starts to decrease. After decreasing linearly in the gain saturation region, it finally approaches an asymptotic value of 0 dB for high input powers. Also shown is the output saturation power, which is the point at which the gain is reduced by 3 dB.

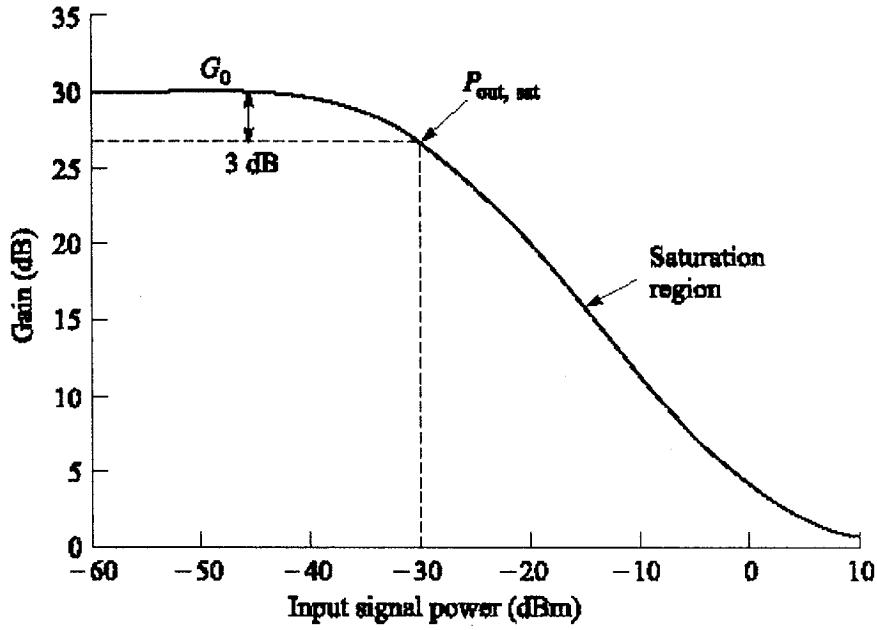

Fig. 2.11 Dependence of the gain on optical input power

The dominant noise generated in an optical amplifier is amplified spontaneous emission (ASE). All amplifiers degrade the signal-to-noise ratio (SNR) of the amplified signal because of spontaneous emission that adds noise to the signal during its amplification. The SNR degradation is quantified through a parameter F_n, called the *amplifier noise figure* and defined as [2]:

$$F_n = \frac{(SNR)_{in}}{(SNR)_{out}} \tag{2.3}$$

where SNR refers to the electric power generated when the optical signal is converted into an electric current.

2.5 Optical and Electrical Filters

The function of optical spectral filters is to recognize a narrow band of optical frequencies from a multiplicity and either pass or reject it, similar to the function of their electrical counterparts. Optical spectral filters are based on *interference* or *absorption* and they are distinguished as *fixed optical filters* or *tunable optical filters*. *Fixed optical filters* are constructed for a specific application and for a specific and narrow slice of the spectrum with specific requirements. As such, although they may have limited applicability, they are simpler and less expensive compared with *tunable optical filters*. *Tunable optical filters* are constructed with passive or active optical components and provide the flexibility to slide window on the optical spectrum [31].

In this thesis, the optical filter is either a Fabry-Perot (FP) filter or a fiber Bragg grating (FBG) filter. For an FP filter, its transfer function $H_o(f)$ is given under the Lorentzian approximation as [32]:

$$H_o(f) = 1/(1 + j2f / B_o) \tag{2.4}$$

where B_o is the 3-dB bandwidth (full width at half height) of the optical filter. For an FBG filter, we have [2]:

$$H_o(f) = \frac{jk \sin[\beta(f) L_g]}{\tanh(kL_g) \times \{\beta(f) \cos[\beta(f) L_g] - j2\pi(f / v_g) \sin[\beta(f) L_g]\}} \tag{2.5}$$

where $\beta(f) = \sqrt{(2\pi f / v_g)^2 - k^2}$, k is the grating coupling coefficient and L_g is the grating length. Owing to technological constraints, the optical bandpass filter following the EDFA to reduce the amplified spontaneous emission (ASE) power at the detector always had to be taken much broader than the bandwidth of the data signal [32]. In this thesis, the optical filter had been assumed to let the data signal pass undistorted.

$H_e(f)$ represents the transfer function of the electrical lowpass filter, which is assumed to be a fifth-order Bessel type and its transfer function is given by [32]:

$$H_e(f) = 945/[jf^5 + 15f^4 - 105jf^3 - 420f^2 + 945jf + 945] \quad (2.6)$$

2.6 Optical Mach-Zehnder Interferometer

The Mach-Zehnder interferometer (MZI) is sketched in Fig. 2.12. The input signal is split into two beams by a 3 dB splitter. In the central section, one of the waveguides is longer by ΔL to give a wavelength dependent phase shift between the two arms. A 3 dB coupler recombines the signals at the output. Briefly speaking, the MZI splits the input beam and introduces a phase shift in one of the paths, and then the recombined signals will interfere constructively at one output port and destructively at the other. The relative phase on recombination determines whether constructive or destructive interference occurs at the output ports.

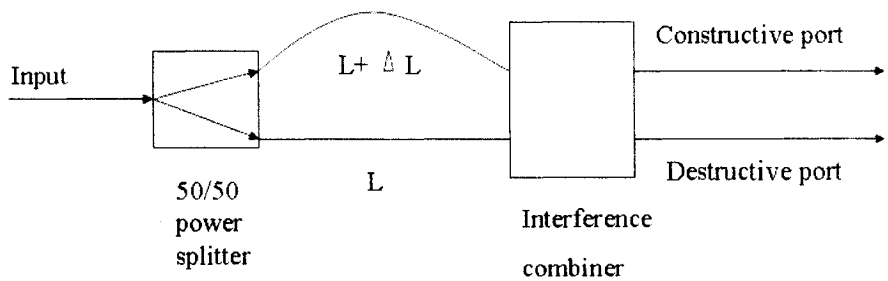

Fig. 2.12 Mach-Zehnder interferometer

In the central section, when the signals in the two arms come from the same light source, the outputs from these two waveguides have a phase difference $\Delta\Phi$ given by [3]:

$$\Delta\Phi = k\Delta L \tag{2.7}$$

where $k = 2\pi n_{eff} / \lambda$, and n_{eff} is the effective refractive index in the waveguide.

In Fig. 2.13 (a), the left two curves represent two light waves traveling along the same path. The two light waves shown are also "in phase". This means the peaks and the valleys of the two waveforms are perfectly aligned. When two light waves have the same wavelength and are in phase, they add together to produce a wave with the sum of the amplitudes of the input waves. This is known as *constructive* interference. If two light waves have the same wavelength but "out of phase", the two input light waves cancel each other, results no output. This is called as *destructive* interference [33]. That is shown in Fig. 2.13 (b).

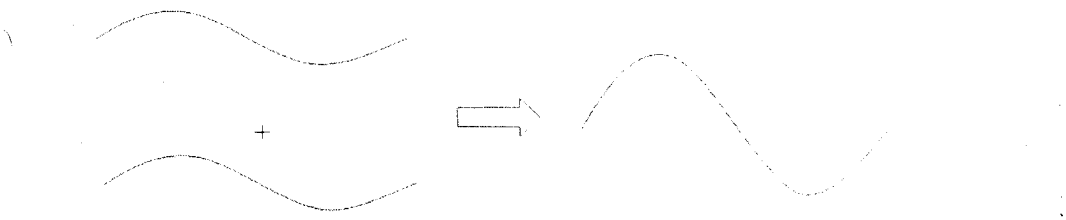

(a) Constructive Interference

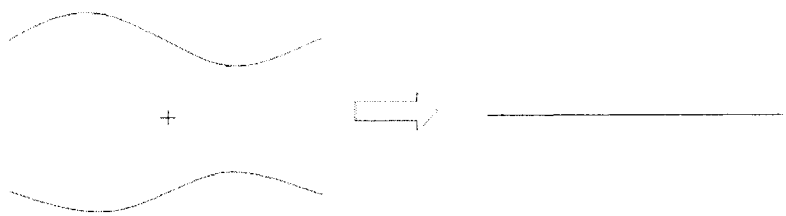

(b) Destructive Interference

Fig. 2.13 Constructive and destructive interference

2.7 Photodetectors

The role of the optical receivers is to convert the optical signal back to electrical form

and recover the data transmitted through the lightwave system. Its main component is a photodetector that works basically in the opposite way to lasers. It should have high sensitivity, fast response, low noise, low cost, and high reliability. Its size should be compatible with the fiber-core size. Although the conversion efficiency actually depends on the complete photoreceiver rather than on the photodetector only, several parameters are used to characterize the ability of the photodetector to meet the requirements of optical fiber transmission: responsivity; bandwidth; and noise characteristics [30]. Although there are several types of photodetectors, not all of them are suitable for use in optical fiber communications systems. In such systems, the optical detector device, which is almost always utilized, is the semiconductor photodiode. Photodetector design criteria are set forth by system parameters such as size, sensitivity, bandwidth, and degree of tolerance to temperature variations. The two photodetector devices most commonly used in optical fiber communications systems are PIN and APD devices.

2.7.1 Receiver Sensitivity

Receiver sensitivity is defined as the average received optical power needed to achieve a given communication rate and performance. For digital systems, the communication rate is measured by the bit rate (R_b) and performance is measured by the bit error ratio (BER) [29].

2.7.2 Shot Noise and Thermal Noise

The shot noise and thermal noise are the fundamental noise contributions in optical receivers. The shot noise is responsible for current fluctuations in all optical receivers

even when the incident optical power is constant. Thermal noise is the result of thermally agitated free-electron motion within any conducting material. At a finite temperature, electrons move randomly in any conductor. Random thermal motion of electrons in a resistor manifests as a fluctuating current even in the absence of an applied voltage [2].

Chapter 3

Dominant Noise Sources

In optically amplified DPSK systems, there are three dominant noise sources: signal-ASE beat noise, ASE-ASE beat noise, and nonlinear phase noise. The first two noise sources are added to the signal, and thus they can be referred to as linearly additive noise. In this chapter, we will introduce some fundamental knowledge and properties of noise sources.

3.1 ASE Beat Noise

The generation of noise in optical amplifiers is, in essence, an effect of the spontaneous deexcitation of the laser ions. As the ions have a finite excited state lifetime, some of the ions spontaneously return to the ground state, thereby emitting a photon. This photon has no coherence characteristics with respect to the incoming signal light, as opposed to a photon generated by stimulated emission. Therefore the collection of such spontaneously generated photons, being multiplied by the fiber amplifier, forms a background noise adding to the signal light. We refer to this background noise as amplified spontaneous emission, or ASE [34].

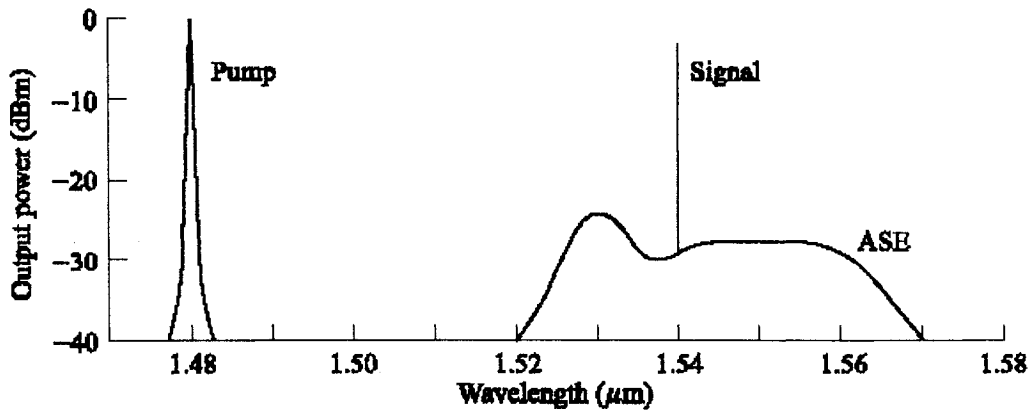

Fig. 3.1 Representative 1480-nm pump spectrum and a typical output signal at 1540nm with the associated ASE noise [3].

ASE is the dominant noise generated in an optical amplifier. The origin of this noise is the spontaneous recombination of electrons and holes in the amplifier medium. This recombination gives rise to a broad spectral background of photons that get amplified along with the optical signal. This effect is shown in Fig. 3.1 for an EDFA amplifying a signal at 1540 nm [3]. The spontaneous noise can be modeled as a stream of random infinitely short pulses that are distributed all along the amplifying medium. Such a random process is characterized by a noise power spectrum that is flat with frequency. The power spectral density of the ASE noise is [3]:

$$N_{ASE}(f) = hvn_{sp}[G(f)-1] = P_{ASE}/B_o \tag{3.1}$$

where P_{ASE} is the ASE noise power in an optical bandwidth B_o and n_{sp} is the spontaneous-emission or population-inversion factor.

Since ASE originates ahead of the photodiode, it gives rise to three different noise components in an optical receiver in addition to the normal thermal noise of the photodetector. This occurs because the photocurrent consists of a number of beat signal

between the signal and the optical noise fields, in addition to the squares of the signal field and the spontaneous-emission field. If the total optical field is the sum of the signal field E_s and the spontaneous-emission field $n(t)$, then the total photodetector current I_{total} is proportional to the square of the electric field of the optical signal: $I_{total} \propto |E_s + n(t)|^2 = |E_s|^2 + |n(t)|^2 + E_s^* n(t) + E_s n^*(t)$, where * represents the conjugated complex. The various components in the ASE noise field will interact with themselves, and we call the second term *ASE-ASE beat noise*. The third and fourth terms are interacting components between the signal and the ASE noise field that are polarized in the same direction as the signal. These are called *signal-ASE beat noise* [3, 7].

3.2 Nonlinear Phase Noise

Differential phase shift keying (DPSK) has recently been the subject of extensive experimental and theoretical studies because DPSK systems have a number of advantages compared to standard intensity modulation and direct detection (IM/DD) systems. However, the performance of DPSK systems may be degraded by the nonlinear phase noise. Nonlinear phase noise is induced by the interaction of amplifier ASE noise and fiber Kerr nonlinearities. The ASE noise induces the signal power fluctuation, and then nonlinear phase shift is generated by *Kerr effect* such as *Self-Phase Modulation* (SPM). Several experiments and simulations already show that the benefit of DPSK receiver with balanced detection is diminished when nonlinear phase noise becomes dominant over linear ASE noise [26, 35]. Nonlinear phase noise causes severe performance degradation in DPSK systems.

3.2.1 What Is SPM

The refractive index of silica was always assumed to be power independent, but in reality all materials behave nonlinearly at high intensities and their refractive index increases with intensity. The refractive index n of many optical materials has a weak dependence on optical intensity *I*, which equals the optical power per effective area in the fiber. The refractive index is given by $n = n_0 + n_2 I = n_0 + n_2 P / A_{eff}$, where n_0 is the ordinary refractive index of the material, n_2 is the nonlinear index coefficient, P is the optical power, and A_{eff} is the effective mode area. In silica, the factor n_2 varies from 2.2 to $3.4 \times 10^8 \mu m^2 / w$. The nonlinearity in the refractive index is known as the Kerr nonlinearity. This nonlinearity produces a carrier-induced phase modulation of the propagating signal, which is called the *Kerr effect*. In single-wavelength links, this gives rise to SPM, which converts optical power fluctuations in a propagating light wave to spurious phase fluctuations in the same wave [3]. SPM is a direct consequence of the refractive index n depending on the power of a pulse, because the speed at which light travels depends on the refractive index [2, 36]. This dynamic characteristic of a propagating optical pulse in fiber results in modulation of its own phase. This nonlinear phenomenon causes spectral broadening [3].

If fiber losses are compensated periodically using optical amplifiers, the nonlinear phase shift Φ_{NL} should be multiplied by the number of amplifier N because the SPM-induced phase accumulates over multiple amplifiers. The nonlinear phase shift is given by [2]

$$\Phi_{NL} = \gamma L_{eff} P_{in} \tag{3.2}$$

where $\gamma = 2\pi\overline{n_2}/(A_{eff}\lambda)$ is the nonlinearity coefficient and L_{eff} is the effective length in the fiber.

3.2.2 Statistical Properties of Nonlinear Phase Noise

Nonlinear phase noise, also called the Gordon-Mollenauer effect, is induced by the interaction of the fiber *Self-Phase Modulation* and optical amplifier ASE noise [37]. Differential phase shift keying (DPSK) signals are degraded by nonlinear phase noise. Recently, Kim and Gnauck show experimentally the nonlinear phase noise is not Gaussian distributed, so the variance or Q factor is not sufficient to characterize the system performance [26]. The probability density function (pdf) of nonlinear phase noise is necessary to better understand the system and evaluates the system performance, and this work was done by Keang-Po Ho [38, 39].

We consider a system with multiple fiber spans using an optical amplifier in each span to compensate for fiber loss. For simplicity, we assume that each span has the same length, and an identical optical power is launched into each span. Here we neglect the effects of dispersion.

For an N span fiber system, the overall nonlinear phase noise is [37]

$$\Phi_{NL} = \gamma L_{eff}\left(|A+n_1|^2 + |A+n_1+n_2|^2 + \ldots + |A+n_1+\ldots+n_N|^2\right) \tag{3.3}$$

where A is a real number that represents the amplitude of the transmitted signal, $n_k = x_k + iy_k$, k=1,...,N, are the optical amplifier noise introduced into the system at the kth fiber span, and n_k are independent identically distributed complex zero-mean Gaussian random variables. γL_{eff} is the product of the fiber's nonlinear coefficient and

the effective fiber length per span.

With large numbers of fiber spans the summation of Eq. (3.3) can be replaced by integration as [38]

$$\Phi_{NL} = k \int_0^L \left| A + S(z) \right|^2 dz \tag{3.4}$$

where $S(z)$ is a zero-mean complex-valued Wiener process or Brownian motion of $E[S(z_1)S^*(z_2)] = \sigma_s^2 \min(z_1, z_2)$ and $k = N\gamma L_{eff} / L$ is the average nonlinear coefficient per unit length. The variance of $\sigma_s^2 = N\sigma_{ASE}^2 / L$ is the noise variance per unit length. $E\left(\left|n_k^2\right|\right) = \sigma_{ASE}^2$, $k = 1,...N$, is the noise variance per amplifier and $E(\ )$ denotes expectation.

The pdf is derived for the following normalized nonlinear phase noise [38]:

$$\phi = \int_0^t \left| \rho + b(t) \right|^2 dt \tag{3.5}$$

where $b(t)$ is a complex Wiener process with an autocorrelation function

$$R_b(t,s) = E[b(s)b^*(t)] = \min(t,s) \tag{3.6}$$

Comparing the integrations of Eq. (3.4) and (3.5), we scale the normalized phase noise by $\phi = L\sigma_s^2 \Phi_{NL} / k$, $t = z / L$ is the normalized distance, $b(t) = S(tL) / \sigma_s / \sqrt{L}$ is the normalized amplifier noise, and $\rho = A / \sigma_s / \sqrt{L}$ is the normalized amplitude. The signal-to noise ratio (SNR) is $\rho^2 = A^2 / (L\sigma_s^2) = A^2 / (N\sigma_{ASE}^2)$.

A brief derivation is provided here to simplify the model. The Wiener process of $b(t)$ can be expanded by use of the standard Karhunen-Loeve expansion [40]:

$$b(t) = \sum_{k=1}^{\infty} \sigma_k x_k \psi_k(t) \tag{3.7}$$

where x_k are independent ideally distributed complex circular Gaussian variables with zero mean and unity variance. The eigenvalues and eigenfunctions of σ_k^2, $\psi_k(t)$, $0 \le t \le 1$ are [40]:

$$\sigma_k = \frac{2}{(2k-1)\pi} \tag{3.8}$$

$$\psi_k(t) = \sqrt{2}\sin\left[\frac{(2k-1)\pi}{2}t\right] \tag{3.9}$$

By using Eq. (3.7-3.9), the normalized phase of Eq.(3.5) is rewritten as [38]

$$\phi = \rho^2 + 2\sqrt{2}\rho\sum_{k=1}^{\infty}\sigma_k^2 R(x_k) + \sum_{k=1}^{\infty}\sigma_k^2 |x_k|^2 \tag{3.10}$$

where $R(\,)$ denotes the real part of a complex number. Because $\sum_{k=1}^{\infty}\sigma_k^2 = 1/2$ [38], we get:

$$\phi = \sum_{k=1}^{\infty}\sigma_k^2 \left|\sqrt{2}\rho + x_k\right|^2 \tag{3.11}$$

The normalized nonlinear phase noise is the summation of infinitely many independently distributed noncentral χ^2 random variables with two degrees of freedom with noncentrality parameters of $2\sigma_k^2\rho^2$ and a variance parameter $\sigma_k^2/2$. The mean and the standard deviation of the random variables are both proportional to the square of the reciprocal of all odd natural numbers. The characteristic function of the normalized phase ϕ of Eq. (3.5) is [38]:

$$\Psi_\phi(jv) = \prod_{k=1}^{\infty}\frac{1}{1-jv\sigma_k^2}\exp\left(\frac{2jv\rho^2\sigma_k^2}{1-jv\sigma_k^2}\right) \tag{3.12}$$

The characteristic function of Eq. (3.5) can be accurately approximated by [38]:

$$\Psi_{\phi}(jv) = \sec(\sqrt{jv}) \exp\left[\rho^2 \sqrt{jv} \tan(\sqrt{jv})\right] \tag{3.13}$$

The pdf of the normalized phase noise is the inverse Fourier transform of the corresponding characteristic function, and is given by

$$f_{\phi}(\phi) = \frac{1}{2\pi} \int_{-\infty}^{\infty} \Psi_{\phi}(jv) e^{-j\phi v} d\phi \tag{3.14}$$

From the characteristic function of Eq. (3.5), the mean normalized nonlinear phase shift is [38]:

$$< \phi >= -j \frac{d}{dv} \Psi_{\phi}(v)|_{v=0} = \rho^2 + \frac{1}{2} \tag{3.15}$$

The scaling from normalized nonlinear phase noise to the nonlinear phase noise is:

$$\Phi_{NL} = \frac{< \Phi_{NL} >}{\rho^2 + 1/2} \phi \tag{3.16}$$

where $< \Phi_{NL} >$ is the mean nonlinear phase shift and is given by [39]:

$$< \Phi_{NL} >= N \gamma L_{eff} [A^2 + (N+1)\sigma^2] \tag{3.17}$$

For simplicity of calculation, $< \Phi_{NL} >= 1 \, radian$ is assumed in this thesis.

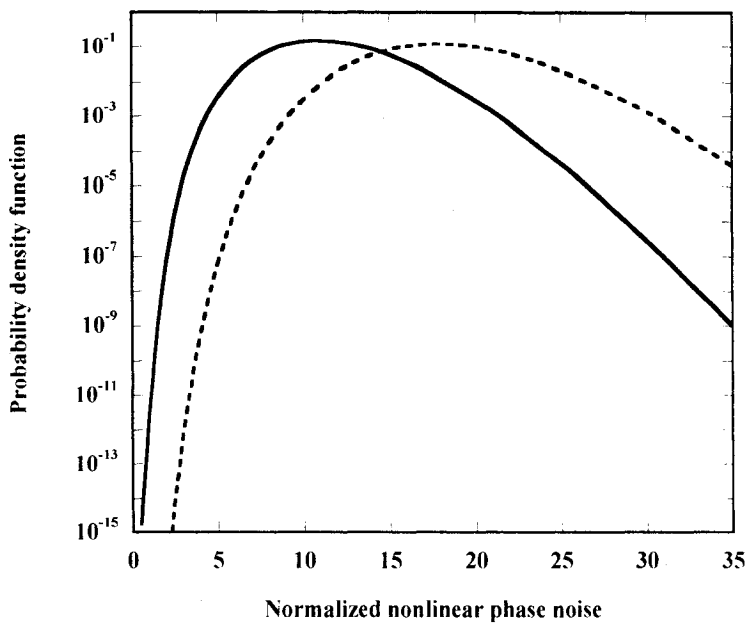

Fig. 3.2 Probability density function of normalized nonlinear phase ϕ for SNR ρ^2 of 11 (solid), and 18 (dashed) [39].

Fig. 3.2 shows the pdf of normalized nonlinear phase. It is obvious that those curves are asymmetrical and they are not Gaussian distribution.

3.2.3 Differential Nonlinear Phase Noise

For DPSK system with Mach-Zehnder interferometer, the effect of nonlinear phase noise is the differential phase between the two arms:

$$\Delta\Phi_{NL} = \Phi_{NL}(t) - \Phi_{NL}(t - T_b) \tag{3.18}$$

Considering the nonlinear phase at t and $t - T_b$ are independent of each other but are identically distributed random variables, where T_b is bit interval. The characteristic

function of the differential phase is given by

$$\Psi_{\Delta\phi}(jv) = \left|\Psi_{\phi}(jv)\right|^2 = \Psi_{\phi}(jv)\Psi_{\phi}^{*}(jv) \tag{3.19}$$

The probability density function can be obtained by taking the inverse Fourier transform of the characteristic function.

$$f_{\Delta\phi}(\Delta\phi) = \frac{1}{2\pi}\int_{-\infty}^{\infty}\Psi_{\Delta\phi}(jv)e^{-j\phi v}d\phi \tag{3.20}$$

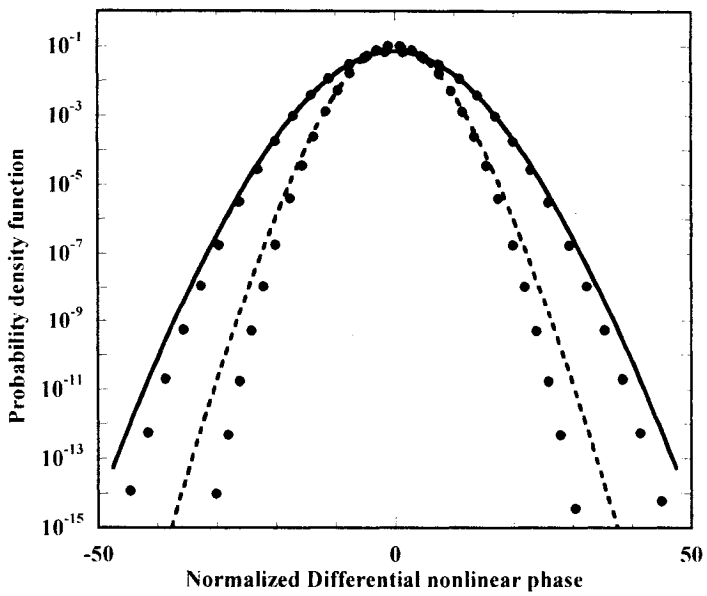

Fig. 3.3 The pdfs of differential nonlinear phase noise $\Delta\phi$ for two cases of $\rho = 11$ (dashed) and $\rho = 25$ (solid), with the Gaussian approximations (dots).

Fig. 3.3 shows the pdfs of the differential nonlinear phase noise. Those curves are also not Gaussian distribution, but they are symmetric and mean is zero. Because the characteristic function of DPSK $\Psi_{\Delta\phi}(jv) = \left|\Psi_{\phi}(jv)\right|^2$ is a real function, the pdf of $\Psi_{\Delta\phi}(jv)$ is an even function. The Gaussian approximations are also given in Fig. 3.3; the

variance of differential nonlinear phase is used by $\sigma_{\Delta\phi}^2 = (4\rho^2 + 1)/3$ [38].

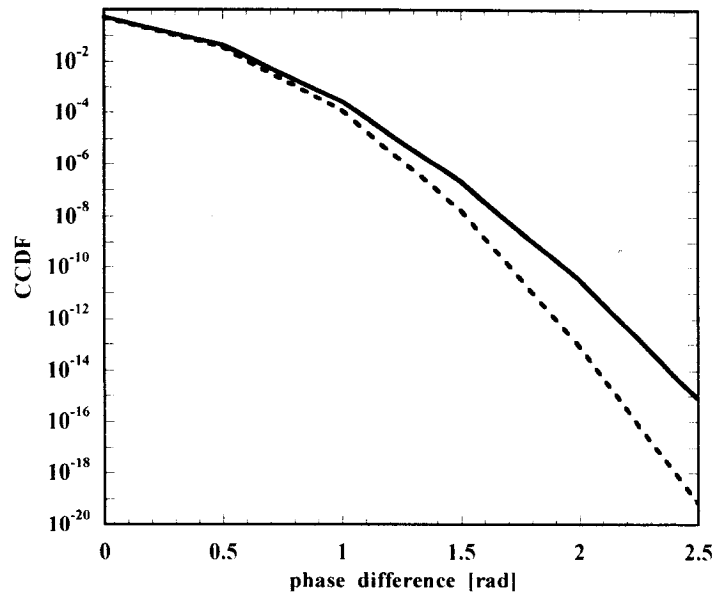

Fig. 3.4 Complementary cumulative distribution function of differential nonlinear phase. exact model (solid) and Gaussian approximation (dashed).

Figure 3.4 shows the complementary cumulative distribution function (CCDF) of the differential nonlinear phase, where $CCDF = 1 - \int_{-\infty}^{\Delta\Phi} f(\Delta\Phi) d\Delta\Phi$. The error probability of nonlinear phase noise is given by twice the CCDF value at $\pi/2$. From Fig. 3.4, it is shown that Gaussian approximation slightly underestimates the impact of nonlinear phase noise.

Chapter 4

Noise Statistic Analysis

For DPSK systems, in-line accumulated ASE noise and nonlinear phase noise are dominant noise, comparing to some fundamental noise such as shot noise and thermal noise, which have small effect and are negligible. The transmitter laser may induce phase noise, but a single-frequency laser is used whose linewidth is negligible in comparison to the symbol rate, so that laser phase noise is negligible. On the contrary, the phase noise almost does not introduce any performance penalty in IM/DD systems.

4.1 Noise Statistic Analysis in IM/DD Receivers

For comparison, we first summarize the noise statistics in IM/DD receivers. This work was done by D. Marcuse [23, 24]. In the intensity-modulation/direct-detection (IM/DD) systems, an electrical bit stream modulates the intensity of an optical carrier inside the optical transmitter and the optical signal transmitted through the fiber link is incident directly on an optical receiver, which converts it to the original digital signal in the electrical domain. The structure of IM/DD system is depicted in Fig.4.1. Procoder and Mach-Zehnder interferometer are not necessary in IM/DD systems.

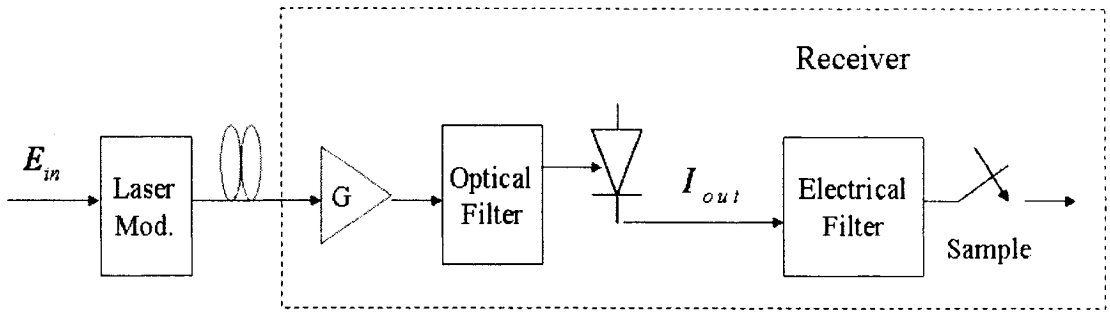

Fig.4.1 Schematic diagram of IM/DD system.

In 1990, D. Marcuse presented a simple derivation of the probability density functions in IM/DD receivers, and he found the exact expressions for the probability density functions are Chi-square distributions [23, 24]. The currents for logical "1" and "0" are given by the expressions as:

$$I_1(t) = R\left|E_1(t) + n(t)\right|^2 = R\left[\left|E_1(t)\right|^2 + E_1(t)n^*(t) + E_1^*(t)n(t) + \left|n(t)\right|^2\right] \quad (4.1)$$

$$I_0(t) = R\left|n(t)\right|^2 \quad (4.2)$$

where R is the *responsivity* of the photodetector, $E_1(t)$ is optical field of optical signal, $n(t)$ is ASE noise. The logical "0" does not carry optical signal power except ASE noise. The pdfs for logical "1" and "0" are given by

$$f_1(x) = \frac{W}{\bar{I}_n}\left(\frac{x}{\bar{I}_1}\right)^{\frac{W-1}{2}} \exp\left(-W\frac{x+\bar{I}_1}{\bar{I}_n}\right) I_{W-1}\left(\frac{2W\sqrt{x\bar{I}_1}}{\bar{I}_n}\right), x \geq 0 \quad (4.3)$$

$$f_0(x) = \left(\frac{W}{\bar{I}_n}\right)^W \frac{x^{W-1}}{\Gamma(W)} \exp\left[-W\frac{x}{\bar{I}_n}\right], x \geq 0 \quad (4.4)$$

where $W = B_o / B_e$, B_o is the optical noise bandwidth of optical filter, B_e is the electrical noise bandwidth of electrical filter. $\bar{I}_1$ is the signal current for logical "1", and

$\overline{I_1} = R|E_1|^2 = 2\overline{I_s}$, where $\overline{I_s}$ is the decision current corresponding to the average power of optical signal, $\overline{I_n}$ is the output current of ASE noise, $I_{W-1}(\ )$ is modified Bessel function, and $\Gamma(\ )$ is Gamma function.

The Gaussian approximations of pdfs for logical "1" and "0" are also given by [23, 24]:

$$f_{g1}(x) = \frac{1}{\sqrt{2\pi}\sigma_1}\exp\left[-\frac{\left(x-\overline{I_1}-\overline{I_n}\right)^2}{2\sigma_1^2}\right] \tag{4.5}$$

$$f_{g0}(x) = \frac{1}{\sqrt{2\pi}\sigma_0}\exp\left[-\frac{\left(x-\overline{I_n}\right)^2}{2\sigma_0^2}\right] \tag{4.6}$$

where $\sigma_1^2 = 8\overline{I_s}(RN_{ASE})B_e + 2R^2N_{ASE}^2(2B_o - B_e)B_e$ is the variance of the noise for logical "1", and $\sigma_0^2 = 2R^2N_{ASE}^2(2B_o - B_e)B_e$ is the variance of the noise for logical "0".

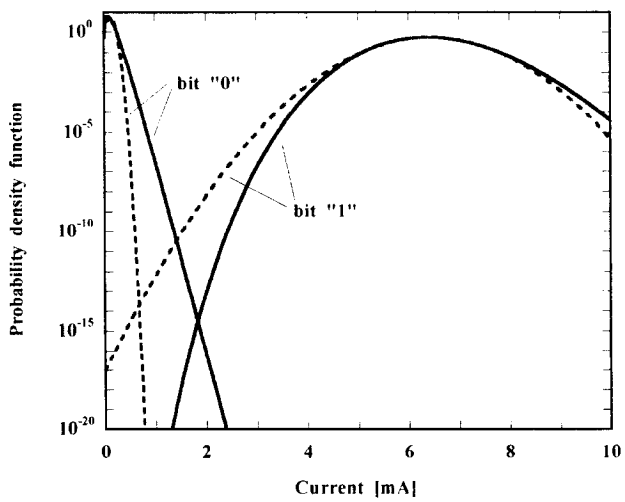

Fig. 4.2 pdfs in IM/DD receivers, the exact pdfs (solid), and Gaussian approximations (dashed).

Fig.4.2 shows the exact pdfs (solid) and Gaussian approximations (dashed) in IM/DD receivers calculated by Eq. (4.3-4.6). We assume bit rate of 43 Gb/s; optical pre-amplifier gain of 35 dB, noise figure of 5 dB, and the average optical signal power of -30 dBm. The other parameters used in this calculation are as follows: B_o=100 GHz, and B_e=33 GHz.

4.2 Noise Statistic Analysis in DPSK Receivers with Balanced Detection

A theoretical analysis of noise statistics in optically pre-amplified DPSK receivers with optical Mach-Zehnder interferometer demodulation is presented for the first time in Section 4.2 and 4.3, and a related research paper was done and submitted for publication [41].

Fig.4.3 shows schematically the process of demodulation in DPSK receivers with balanced detection. The input signal E_0 is split into E_1 and E_2 by a 3 dB splitter. In the central section, one of the waveguides is longer by ΔL to give a time delay τ between the two arms, which equals one bit interval, and $\tau = 1/R_b$ (R_b is the bit rate). The optical fields of outputs at the constructive and destructive ports are the sum and difference of optical fields on two arms. Maximum power appears at the constructive port when there is no phase change between adjacent bits and at the destructive port when the phase in adjacent bits differs by π. This is the reason why an electronic precoder is needed before the transmitter. A balanced optical receiver yields a photocurrent proportional to the difference between the intensities at the two interferometer output ports.

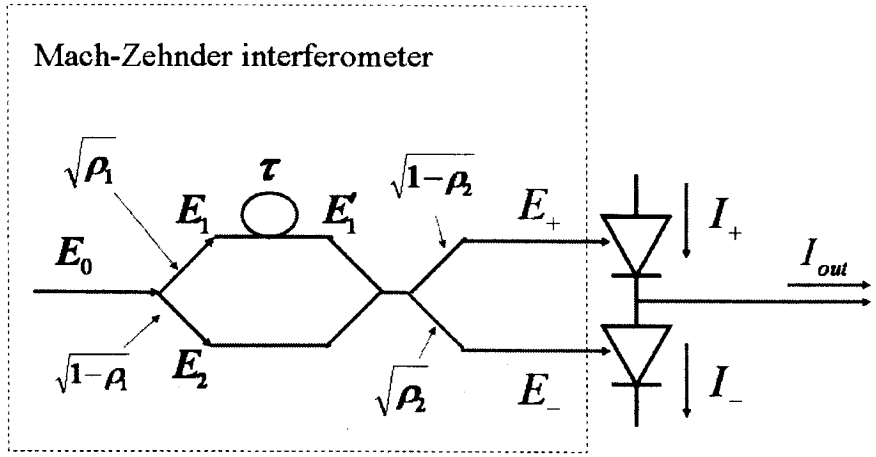

Fig. 4.3 Schematic diagram of DPSK receivers with balanced detection

$$E_1 = \sqrt{\rho_1} E_0 \tag{4.7}$$

$$E_2 = -j\sqrt{1-\rho_1} E_0 \tag{4.8}$$

$$E_1' = \sqrt{\rho_1} E_0(t-\tau) \tag{4.9}$$

$$\begin{bmatrix} E_- \\ E_+ \end{bmatrix} = \begin{bmatrix} \sqrt{\rho_2} & -j\sqrt{1-\rho_2} \\ -j\sqrt{1-\rho_2} & \sqrt{\rho_2} \end{bmatrix} \begin{bmatrix} E_1' \\ E_2 \end{bmatrix} \tag{4.10}$$

where ρ_1 and ρ_2 are power splitting ratio of two optical couplers. For the ideal 3 dB couplers, $\rho_1 = \rho_2 = 1/2$, we simplify Eq.(4.10) as follows:

$$E_-(t) = \frac{1}{2}\left[E_0(t-\tau) - E_0(t)\right] \tag{4.11}$$

$$E_+(t) = \frac{-j}{2}\left[E_0(t-\tau) + E_0(t)\right] \tag{4.12}$$

The input of MZI $E_0(t)$ is given by

$$E_0(t) = E_s(t) e^{j\theta(t)+j\Phi(t)} + n(t) \tag{4.13}$$

where $E_s(t)$ represents the amplitude modulation of optical signal, and it is assumed as

real number, $\theta(t)$ denotes the phase modulation of the DPSK signal, $\Phi(t)$ is the nonlinear phase noise, and $n(t)$ represents ASE noise. The output currents are given by

$$I_+ = R\left|E_+\right|^2 = R\left|E_{s+} + n_+(t)\right|^2 \tag{4.14}$$

$$I_- = R\left|E_-\right|^2 = R\left|E_{s-} + n_-(t)\right|^2 \tag{4.15}$$

$$I_{out} = I_+ - I_- \tag{4.16}$$

where E_{s+} and E_{s-} denote the transmitted signal at the constructive and destructive ports, respectively. $n_+(t)$ and $n_-(t)$ represent the ASE noise at the constructive and destructive ports, respectively.

Usually the condition of $E_s(t-\tau) \approx E_s(t) = E_s$ always holds, thus we obtain:

$$E_{s+} = \frac{-j}{2}\left[E_s(t-\tau)e^{j\theta(t-\tau)+j\Phi(t-\tau)} + E_s(t)e^{j\theta(t)+j\Phi(t)}\right]$$

$$= \frac{-j}{2}E_s e^{j\theta(t)+j\Phi(t)}\left[e^{j\Delta\theta+j\Delta\Phi}+1\right] \tag{4.17}$$

$$n_+(t) = \frac{-j}{2}\left[n(t-\tau)+n(t)\right] \tag{4.18}$$

$$E_{s-} = \frac{1}{2}\left[E_s(t-\tau)e^{j\theta(t-\tau)+j\Phi(t-\tau)} - E_s(t)e^{j\theta(t)+j\Phi(t)}\right]$$

$$= \frac{1}{2}E_s e^{j\theta(t)+j\Phi(t)}\left[e^{j\Delta\theta+j\Delta\Phi}-1\right] \tag{4.19}$$

$$n_-(t) = \frac{1}{2}\left[n(t-\tau)-n(t)\right] \tag{4.20}$$

where $\Delta\theta$ represents the phase difference between two successive bits, and $\Delta\Phi$ represents the differential nonlinear phase between the two arms of MZI.

For logical "1", there is no phase change between two successive bits, that is $\Delta\theta = 0$.

The signal current at the constructive port is given by

$$\overline{I_+} = R\left|E_{s+}\right|^2$$

$$= R\left|\frac{-j}{2}E_s e^{j\theta(t)+j\Phi(t)}\left[e^{j\Delta\theta+j\Delta\Phi}+1\right]\right|^2$$

$$= R\left|E_s\right|^2\left|\frac{1+e^{j\Delta\Phi}}{2}\right|^2$$

$$= R\left|E_s\right|^2\frac{1+\cos(\Delta\Phi)}{2} \tag{4.21}$$

In DPSK systems, bit "1" and "0" carry the same optical power, so the decision current which is corresponding to the average transmitted optical power is given by

$$\overline{I_s} = R\left|E_s\right|^2 \tag{4.22}$$

then

$$\overline{I_+} = \frac{1+\cos(\Delta\Phi)}{2}\overline{I_s} \tag{4.23}$$

The signal current at the destructive port for logical "1" is given by

$$\overline{I_-} = R\left|E_{s-}\right|^2$$

$$= R\left|\frac{1}{2}E_s e^{j\theta(t)+j\Phi(t)}\left[e^{j\Delta\Phi}-1\right]\right|^2$$

$$= R\left|E_s\right|^2\frac{1-\cos(\Delta\Phi)}{2}$$

$$= \frac{1-\cos(\Delta\Phi)}{2}\overline{I_s} \tag{4.24}$$

The output currents for logical "1" are given by

$$I_+ = R|E_+|^2$$

$$= R|E_{s+} + n_+(t)|^2$$

$$= R\left[|E_{s+}|^2 + E_{s+}n_+^*(t) + E_{s+}^* n_+(t) + |n_+(t)|^2\right]$$

$$= \frac{1+\cos(\Delta\Phi)}{2}\overline{I_s} + R\left[E_{s+}n_+^*(t) + E_{s+}^* n_+(t) + |n_+(t)|^2\right] \quad (4.25)$$

$$I_- = R|E_-|^2$$

$$= R|E_{s-} + n_-(t)|^2$$

$$= R\left[|E_{s-}|^2 + E_{s-}n_-^*(t) + E_{s-}^* n_-(t) + |n_-(t)|^2\right]$$

$$= \frac{1-\cos(\Delta\Phi)}{2}\overline{I_s} + R\left[E_{s-}n_-^*(t) + E_{s-}^* n_-(t) + |n_-(t)|^2\right] \quad (4.26)$$

$$I_1 = I_+ - I_-$$

$$= \overline{I_s}\cos(\Delta\Phi) + R\left[E_{s+}n_+^*(t) + E_{s+}^* n_+(t) + |n_+(t)|^2\right] - R\left[E_{s-}n_-^*(t) + E_{s-}^* n_-(t) + |n_-(t)|^2\right]$$

$$\approx \overline{I_s}\cos(\Delta\Phi) + R\left[E_{s+}n_+^*(t) + E_{s+}^* n_+(t)\right] + R|n_+(t)|^2 - R\left[|n_-(t)|^2\right] \quad (4.27)$$

where the two terms $E_{s+}n_+^*(t)$ and $E_{s+}^* n_+(t)$ are referred to as signal-ASE beat noise at the constructive port, the two terms $E_{s-}n_-^*(t)$ and $E_{s-}^* n_-(t)$ are referred to as signal-ASE beat noise at the destructive port, $|n_+(t)|^2$ and $|n_-(t)|^2$ are referred to as ASE-ASE beat noise at the constructive and destructive ports, respectively, and * represents the complex conjugation.

The conditional pdf of the first three terms in Eq. (4.27), which are from the constructive port, is Chi-square distribution and given by (see detailed derivation in

Appendix A)

$$f_+(x|\Delta\Phi)=\frac{M}{\bar{I}_m}\left(\frac{x}{\bar{I}_1}\right)^{\frac{M-1}{2}}\exp\left(-M\frac{x+\bar{I}_1}{\bar{I}_m}\right)I_{M-1}\left(\frac{2M\sqrt{x\bar{I}_1}}{\bar{I}_m}\right),x\geq 0 \qquad (4.28)$$

where $M=B_o/B_e$, $\bar{I}_1=\bar{I}_s\cos(\Delta\Phi)$ is the signal current, $\bar{I}_m=2RN_{ASE}B_+$ is the output current of ASE noise at the constructive port, $B_+=B_o/2+\sin(\pi B_oT_b)/(2\pi T_b)$ is the equivalent optical noise bandwidth after the MZI at the constructive port (see Appendix B), T_b is bit period, and N_{ASE} is the power density of ASE noise at one polarization state.

The pdf for the last term $\left(R|n_-(t)|^2\right)$ in Eq.(4.27), which is from the destructive port, is also Chi-square distribution and is given by (see detailed derivation in Appendix A)

$$f_-(y)=\left(\frac{M}{\bar{I}_n}\right)^M\frac{y^{M-1}}{\Gamma(M)}\exp\left[-M\frac{y}{\bar{I}_n}\right],y\geq 0 \qquad (4.29)$$

where $\bar{I}_n=2RN_{ASE}B_-$ is the output current of ASE noise at the destructive port, $B_-=B_o/2-\sin(\pi B_oT_b)/(2\pi T_b)$ is the equivalent optical noise bandwidth after the MZI at the destructive port (see Appendix B).

Considering x and y in Eq. (4.28) and (4.29) are two independent random variables, the pdf of $z=x-y$ is given by $f(z)=\int_{-\infty}^{\infty}f_x(z+y)f_y(y)dy$. The conditional pdf of I_1 in Eq.(4.27) is given by

$$f_1(x|\Delta\Phi)=\int_0^{\infty}f_+\left[(x+y)|\Delta\Phi\right]f_-(y)dy \qquad (4.30)$$

This integral in Eq. (4.30) is the convolution of the functions $f_+(x|\Delta\Phi)$ and $f_-(y)$

from Eq. (4.28) and (4.29). If both linearly additive ASE noise and nonlinear phase noise are taken into account, and we assume the nonlinear phase noise is an independent random variable, the total pdf of output current for logical "1" is obtained as

$$f_1(x)=\int_{-\infty}^{\infty} f_{\Delta\Phi}(\Delta\Phi) f_1(x|\Delta\Phi)\, d\Delta\Phi \tag{4.31}$$

where $f_{\Delta\Phi}(\Delta\Phi)$ is the pdf of differential nonlinear phase $\Delta\Phi$, and can be obtained from Section 3.2.3.

The derivation of pdf for logical "0" may follow the same steps above. For logical "0", there is π phase shift between two adjacent bits, that is $\Delta\theta=\pi$. The output currents are given by

$$I_+ = \frac{1-\cos(\Delta\Phi)}{2}\overline{I_s} + R\left[E_{s+}n_+^*(t)+E_{s+}^* n_+(t)+|n_+(t)|^2\right] \tag{4.32}$$

$$I_- = \frac{1+\cos(\Delta\Phi)}{2}\overline{I_s} + R\left[E_{s-}n_-^*(t)+E_{s-}^* n_-(t)+|n_-(t)|^2\right] \tag{4.33}$$

$$\begin{aligned} I_0 &= I_+ - I_- \\ &\approx -\overline{I_s}\cos(\Delta\Phi) - R\left[E_{s-}n_-^*(t)+E_{s-}^* n_-(t)\right] - R\left[|n_-(t)|^2\right] + R|n_+(t)|^2 \end{aligned} \tag{4.34}$$

The pdf for the last term($R|n_+(t)|^2$)in Eq.(4.34), which is from the constructive port, is given by

$$f_+(x)=\left(\frac{M}{\overline{I_m}}\right)^M \frac{x^{M-1}}{\Gamma(M)}\exp\left[-M\frac{x}{\overline{I_m}}\right], x\ge 0 \tag{4.35}$$

The conditional pdf of the first three terms in Eq. (4.34) which are from the destructive port $\left(\overline{I_s}\cos(\Delta\Phi)+R\left[E_{s-}n_-^*(t)+E_{s-}^* n_-(t)\right]+R\left[|n_-(t)|^2\right]\right)$, is Chi-square distribution and given by

$$f_{-}(y|\Delta\Phi)=\frac{M}{\bar{I}_n}\left(\frac{y}{\bar{I}_0}\right)^{\frac{M-1}{2}}\exp\left(-M\frac{y+\bar{I}_0}{\bar{I}_n}\right)I_{M-1}\left(\frac{2M\sqrt{y\bar{I}_0}}{\bar{I}_n}\right),y\geq 0 \tag{4.36}$$

where $M=B_o/B_e$, $\bar{I}_0=\bar{I}_s\cos(\Delta\Phi)$ is the signal current for logical "0", $\bar{I}_m=2RN_{ASE}B_+$ and $\bar{I}_n=2RN_{ASE}B_-$ are the output currents of ASE noise at the constructive and destructive ports, respectively. $B_+=B_o/2+\sin(\pi B_oT_b)/(2\pi T_b)$ and $B_-=B_o/2-\sin(\pi B_oT_b)/(2\pi T_b)$ are the equivalent optical noise bandwidth after the MZI at the constructive and destructive ports, respectively (see Appendix B). T_b is bit period, and N_{ASE} is the power density of ASE noise at one polarization state.

The conditional pdf and total pdf of logical "0" are given by

$$f_0(x|\Delta\Phi)=\int_0^{\infty}f_{+}(x+y)f_{-}(y|\Delta\Phi)dy \tag{4.37}$$

$$f_0(x)=\int_{-\infty}^{\infty}f_{\Delta\Phi}(\Delta\Phi)f_0(x|\Delta\Phi)d\Delta\Phi \tag{4.38}$$

where $f_{+}(x)$ and $f_{-}(y|\Delta\Phi)$ can be obtained from Eq. (4.35) and (4.36), $f_{\Delta\Phi}(\Delta\Phi)$ is the pdf of differential nonlinear phase $\Delta\Phi$, and can be obtained from Section 3.2.3.

For further studying the DPSK receivers, the comparison of exact pdfs to Gaussian approximations is given. The pdfs for logical "1" and "0" in Gaussian approximations are given by

$$f_{1g}(x)=\int_{-\infty}^{\infty}f_{\Delta\Phi}(\Delta\Phi)\frac{1}{\sqrt{2\pi}\sigma_1}\exp\left[-\frac{\left(x-\bar{I}_1-\bar{I}_m-\bar{I}_n\right)^2}{2\sigma_1^2}\right]d\Delta\Phi \tag{4.39}$$

$$f_{0g}(y) = \int_{-\infty}^{\infty} f_{\Delta\Phi}(\Delta\Phi)\frac{1}{\sqrt{2\pi}\sigma_0}\exp\left[-\frac{\left(y+\overline{I_0}+\overline{I_m}+\overline{I_n}\right)^2}{2\sigma_0^2}\right]d\Delta\Phi \tag{4.40}$$

$$\sigma_1^2 = \sigma_0^2 = \sigma_{SA}^2 + \sigma_{AA+}^2 + \sigma_{AA-}^2 = 2\overline{I_s}RN_{ASE}B_e + R^2N_{ASE}^2(B_o - B_e)B_e \tag{4.41}$$

where σ_{SA}^2 is the variance of signal-ASE beat noise, σ_{AA+}^2 and σ_{AA-}^2 are the variance of ASE-ASE beat noise at the constructive and destructive ports, respectively. $\overline{I_1} = \overline{I_0} = \overline{I_s}\cos(\Delta\Phi)$ are the signal currents for logical "1" and "0", $\overline{I_m} = 2RN_{ASE}B_+$ and $\overline{I_n} = 2RN_{ASE}B_-$ are the output currents of ASE noise at the constructive and destructive ports, respectively. $B_+ = B_o/2 + \sin(\pi B_o T_b)/(2\pi T_b)$ and $B_- = B_o/2 - \sin(\pi B_o T_b)/(2\pi T_b)$ are the equivalent optical noise bandwidth after the MZI at the constructive and destructive ports, respectively (see Appendix B). T_b is bit period, and N_{ASE} is the power density of ASE noise at one polarization state.

In order to figure out the impact of linear ASE noise and nonlinear phase noise on the pdfs, we depict the pdfs for two extreme cases in Fig. 4.4 and 4.5. Fig. 4.4 shows the exact pdfs (solid) and Gaussian approximations (dashed) for logical "1" and "0" without the impact of nonlinear phase noise. It is observed that the exact pdfs are not symmetrical to the mean of the current. The detection threshold for balanced receiver is always zero. The parameters used in this calculation are the same as in Fig. 4.2.

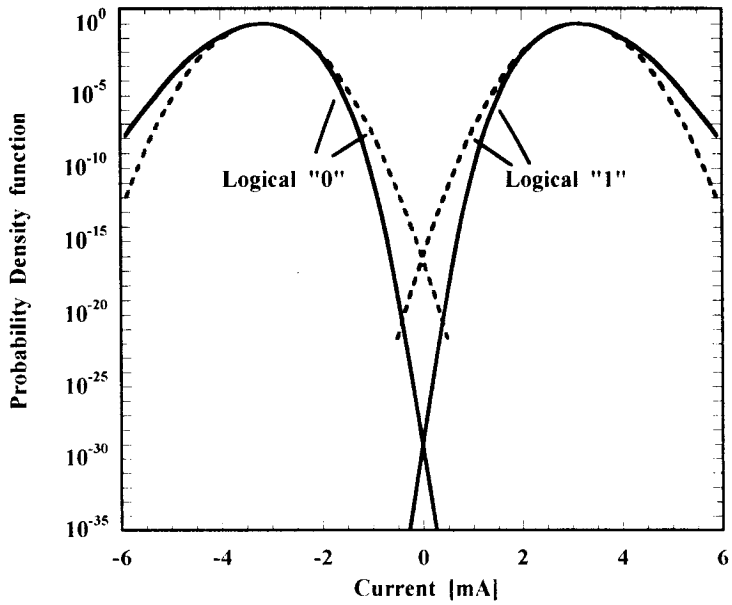

Fig. 4.4 The exact pdfs (solid) and Gaussian approximations (dashed) for DPSK receivers with balanced detection without the impact of nonlinear phase noise.

Fig. 4.5 shows the exact pdfs (solid) and Gaussian approximations (dashed) for logical "1" and "0" with the significant impact of nonlinear phase noise. The parameters used in this calculation are the same as in Fig. 4.2 except noise figure of 3 dB, and $\rho^2 = 25$ in $f_{\Delta\Phi}(\Delta\Phi)$ for calculating the impact of nonlinear phase noise.

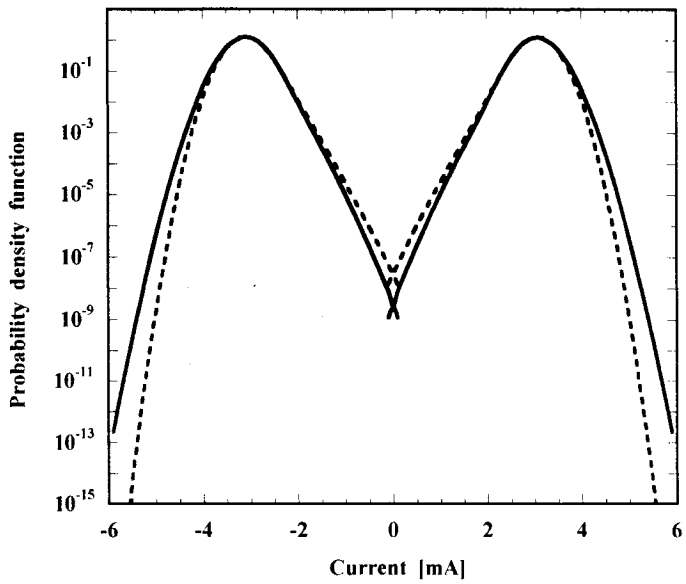

Fig.4.5 The exact pdfs (solid) and Gaussian approximations (dashed) with the significant impact of nonlinear phase noise in DPSK receivers with balanced detection.

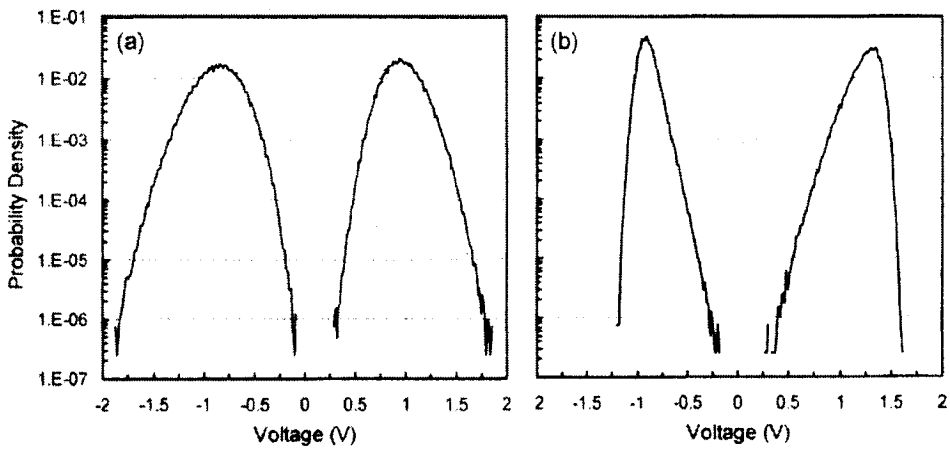

Fig 4.6 Measured voltage histograms when the system performance is limited by (a) linear noise and (b) nonlinear phase noise [35].

The shape of calculated pdfs in Fig. 4.4 and 4.5 are in good agreement with the experimental measured results in Fig. 4.6 [35]. There is noticeable difference in the inner tails of pdfs in Fig. 4.4 and 4.5. This difference is very important to the receiver performance since the inner tails of the pdfs determine the BER. The nonlinear phase noise limits the performance of DPSK systems and the benefit of the balanced receiver is diminished as nonlinear phase noise becomes dominant over linear ASE noise. For comparison, both in Fig. 4.4 and 4.5, the inner tails of the pdfs in the Gaussian approximation overestimate the BER. In order to further prove nonlinear phase noise may degrade the performance of DPSK receivers with balanced detection and Gaussian approximation overestimate the BER, we calculate BER by

$$BER = \frac{1}{2}\left[\int_{I_{th}}^{\infty} f_0(x)dx + \int_{-\infty}^{I_{th}} f_1(x)dx\right] \tag{4.42}$$

where $f_1(x)$ and $f_0(x)$ are the pdfs for logical "1" and "0" respectively, I_{th} is decision current threshold and always equals zero for DPSK receiver with balanced detection.

Fig. 4.7 shows bit error rate without the impact of nonlinear phase noise for DPSK receivers with balanced detection and IM/DD receivers. The parameters used in this calculation are the same as in Fig. 4.2 except we change the average optical signal power within the range from -40 dBm to -32 dBm.

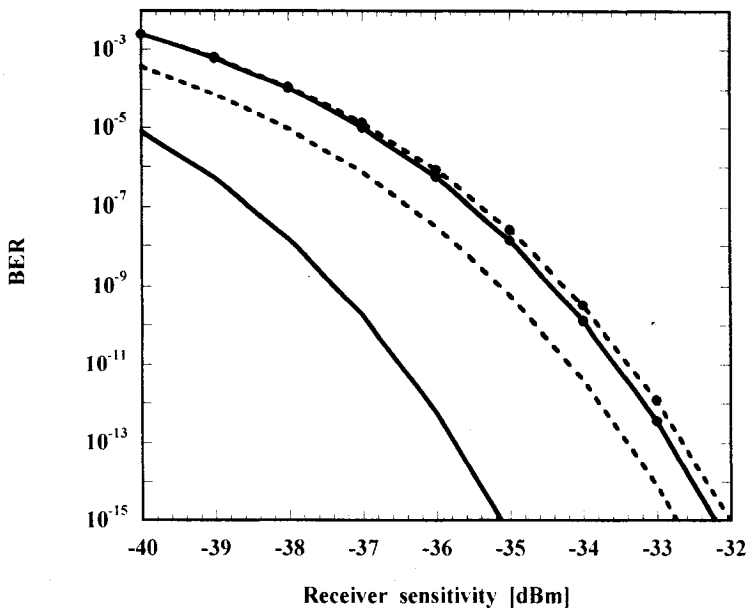

Fig.4.7 BER without the impact of nonlinear phase noise for DPSK receivers with balanced detection calculated by the exact pdfs (solid) and Gaussian approximations (dashed). BER for IM/DD receivers calculated by the exact pdfs (solid with dots) and Gaussian approximations (dashed with dots).

In Fig.4.7, when the BER equals 10^{-9}, the required receiver sensitivity for DPSK receivers with balanced detection is 3 dB lower than that for IM/DD receivers when the exact pdfs are used to calculate BER. However, only 1 dB improvement can be obtained by Gaussian approximations, which strongly overestimate the BER and induce about 2 dB under-estimation of improvement on receiver sensitivity. It is concluded that the conventional Gaussian approximation is not adequate for DPSK receivers with balanced detection.

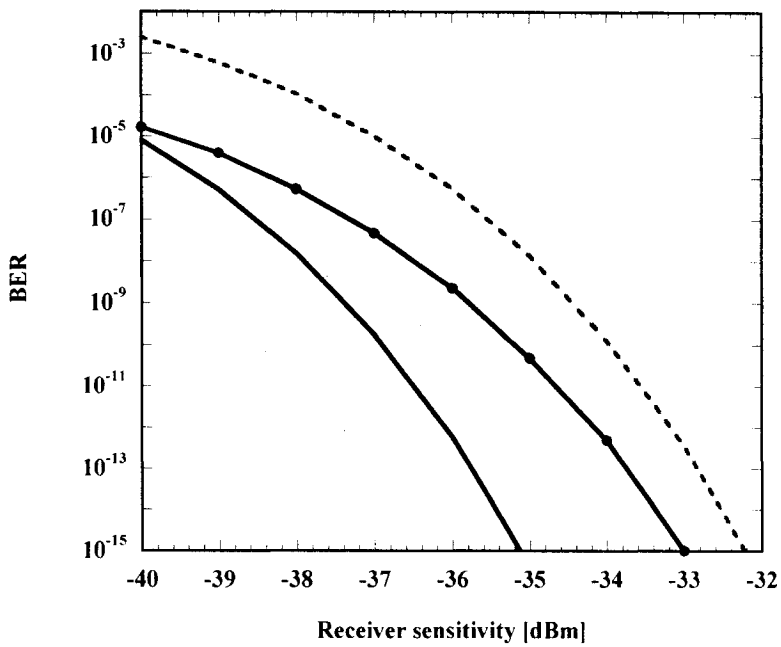

Fig. 4.8 BER for DPSK receivers with balanced detection without the impact of nonlinear phase noise (solid), and with the significant impact of nonlinear phase noise(solid with dots), BER for IM/DD receivers (dashed).

Fig 4.8 shows BER with and without the impact of nonlinear phase noise for DPSK receivers with balanced detection, and also shows BER for IM/DD receivers. From Fig. 4.8, it is concluded that the benefit of DPSK receiver with balanced detection is diminished if nonlinear phase noise becomes dominant over linear noise. $\rho^2 = 25$ is used to calculate the impact of nonlinear phase noise in $f_{\Delta\Phi}(\Delta\Phi)$.

4.3 Noise Statistic Analysis in DPSK Receivers with Single-port Detection

For single-port detection, we only use one port, which is either constructive or destructive port. We assume that the constructive port is used below. Fig.4.9 shows the schematic diagram of DPSK receivers with constructive-port detection.

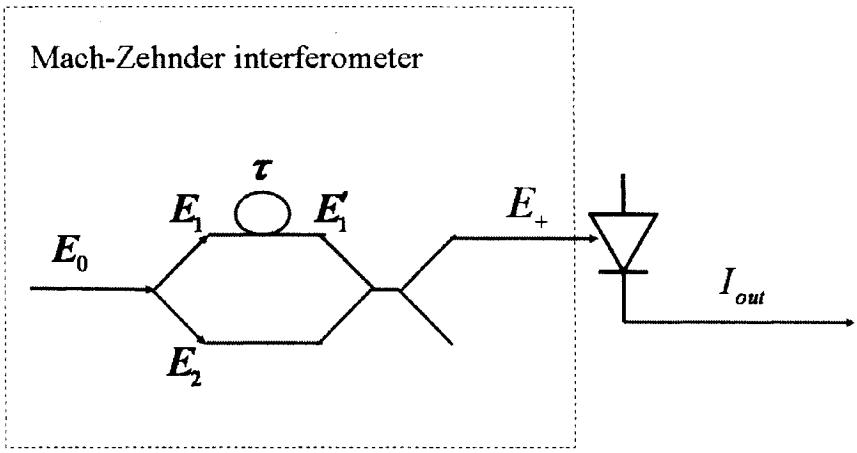

Fig.4.9 Schematic diagram of DPSK receivers with single-port detection

For logical "1", there is no phase shift between the two adjacent bits. that is $\Delta\theta = 0$. and then the optical field on the constructive port is given by

$$E_{s+} = \frac{-j}{2} E_s e^{j\theta(t)+j\Phi(t)}\left[e^{j\Delta\theta+j\Delta\Phi}+1\right]$$

$$= \frac{-j}{2} E_s e^{j\theta(t)+j\Phi(t)}\left[e^{j\Delta\Phi}+1\right] \tag{4.43}$$

The signal current for logical "1" is given by

$$\overline{I_1} = R\left|E_{S+}\right|^2$$

$$= R\left|E_s\right|^2 \frac{1+\cos(\Delta\Phi)}{2}$$

$$= \overline{I_s}\frac{1+\cos(\Delta\Phi)}{2} \tag{4.44}$$

The output current for logical "1" is given by

$$I_1(t) = R\left|E_{s+} + n_+(t)\right|^2$$

$$= \bar{I}_s \frac{1+\cos(\Delta\Phi)}{2} + R\left[E_{s+}^* n_+(t) + E_{s+} n_+^*(t) + \left|n_+(t)\right|^2\right] \tag{4.45}$$

The conditional and total pdfs of output current for logical "1" with constructive-port detection are given by (see detailed derivation in Appendix A)

$$f_1(x|\Delta\Phi) = \frac{M}{\bar{I}_m}\left(\frac{x}{\bar{I}_1}\right)^{\frac{M-1}{2}} \exp\left(-M\frac{x+\bar{I}_1}{\bar{I}_m}\right) I_{M-1}\left(\frac{2M\sqrt{x\bar{I}_1}}{\bar{I}_m}\right), x \geq 0 \tag{4.46}$$

$$f_1(x) = \int_{-\infty}^{\infty} f_{\Delta\Phi}(\Delta\Phi) f_1(x|\Delta\Phi)\, d\Delta\Phi \tag{4.47}$$

where $M = B_o / B_e$, $f_{\Delta\Phi}(\Delta\Phi)$ is the pdf of differential nonlinear phase $\Delta\Phi$, and can be obtained from Section 3.2.3, $\bar{I}_1 = \frac{1+\cos(\Delta\Phi)}{2}\bar{I}_s$ is the signal current for logical "1", $\bar{I}_s$ is the decision current which is corresponding to the average transmitted optical power, $\bar{I}_m = 2RN_{ASE}B_+$ is the output currents of ASE noise at the constructive port. $B_+ = B_o/2 + \sin(\pi B_o T_b)/(2\pi T_b)$ is the equivalent optical noise bandwidth after the MZI at the constructive port (see Appendix B). T_b is bit period, and N_{ASE} is the power density of ASE noise at one polarization state.

For logical "0", there is π phase shift between the two adjacent bits, that is $\Delta\theta = \pi$, and then the optical field on the constructive port is given by

$$E_{s+} = \frac{-j}{2} E_s e^{j\theta(t)+j\Phi(t)} \left[e^{j\Delta\theta + j\Delta\Phi} + 1 \right]$$

$$= \frac{-j}{2} E_s e^{j\theta(t)+j\Phi(t)} \left[e^{j(\Delta\Phi+\pi)} + 1 \right] \tag{4.48}$$

The signal current for logical "0" is given by

$$\overline{I_0} = R\left|E_{S+}\right|^2$$

$$= R\left|E_s\right|^2 \frac{1-\cos(\Delta\Phi)}{2}$$

$$= \overline{I_s} \frac{1-\cos(\Delta\Phi)}{2} \tag{4.49}$$

The output current for logical "0" is given by

$$I_0(t) = R\left|E_{s+} + n_+(t)\right|^2$$

$$= \overline{I_s} \frac{1-\cos(\Delta\Phi)}{2} + R\left[E_{s+}^* n_+(t) + E_{s+} n_+^*(t) + \left|n_+(t)\right|^2 \right] \tag{4.50}$$

The conditional and total pdfs of output current for logical "0" with constructive-port detection are given by (see detailed derivation in Appendix A)

$$f_0(x\left|\Delta\Phi\right.) = \frac{M}{\overline{I_m}} \left(\frac{x}{\overline{I_0}} \right)^{\frac{M-1}{2}} \exp\left(-M \frac{x+\overline{I_0}}{\overline{I_m}} \right) I_{M-1}\left(\frac{2M\sqrt{x\overline{I_0}}}{\overline{I_m}} \right), x \geq 0 \tag{4.51}$$

$$f_0(x) = \int_{-\infty}^{\infty} f_{\Delta\Phi}(\Delta\Phi) f_0\left(x\left|\Delta\Phi\right.\right) d\Delta\Phi \tag{4.52}$$

where $M = B_o / B_e$, $f_{\Delta\Phi}(\Delta\Phi)$ is the pdf of differential nonlinear phase $\Delta\Phi$, and can be obtained from Section 3.2.3, $\overline{I_0} = \frac{1-\cos(\Delta\Phi)}{2}\overline{I_s}$ is the signal current for bit "0", $\overline{I_s}$ is the decision current which is corresponding to the average transmitted optical power.

$\overline{I}_m = 2RN_{ASE}B_+$ is the output currents of ASE noise at the constructive port. $B_+ = B_o/2 + \sin(\pi B_o T_b)/(2\pi T_b)$ is the equivalent optical noise bandwidth after the MZI at the constructive port (see Appendix B). T_b is bit period, and N_{ASE} is the power density of ASE noise at one polarization state.

For comparison, the conventional Gaussian model is given below. The pdfs for logical "1" and "0" in Gaussian approximations are given by

$$f_{1g}(x) = \int_{-\infty}^{\infty} f_{\Delta\Phi}(\Delta\Phi)\frac{1}{\sqrt{2\pi}\sigma_1}\exp\left[-\frac{\left(x-\overline{I}_1-\overline{I}_m\right)^2}{2\sigma_1^2}\right]d\Delta\Phi \tag{4.53}$$

$$f_{0g}(y) = \frac{1}{\sqrt{2\pi}\sigma_0}\exp\left[-\frac{\left(y-\overline{I}_0-\overline{I}_m\right)^2}{2\sigma_0^2}\right] \tag{4.54}$$

$$\sigma_1^2 = \sigma_{SA}^2 + \sigma_{AA}^2 = 2\overline{I}_s RN_{ASE}B_e + R^2N_{ASE}^2(2B_+ - B_e)B_e \tag{4.55}$$

$$\sigma_0^2 = \sigma_{AA}^2 = R^2N_{ASE}^2(2B_+ - B_e)B_e \tag{4.56}$$

where $\overline{I}_1 = \frac{1}{2}\overline{I}_s\left[1+\cos(\Delta\Phi)\right]$, $\overline{I}_0 = \frac{1}{2}\overline{I}_s\left[1-\cos(\Delta\Phi)\right]$, $\overline{I}_m = 2RN_{ASE}B_+$ is the output currents of ASE noise at the constructive port. $B_+ = B_o/2 + \sin(\pi B_o T_b)/(2\pi T_b)$ is the equivalent optical noise bandwidth after the MZI at the constructive port (see Appendix B). T_b is bit period, and N_{ASE} is the power density of ASE noise at one polarization state.

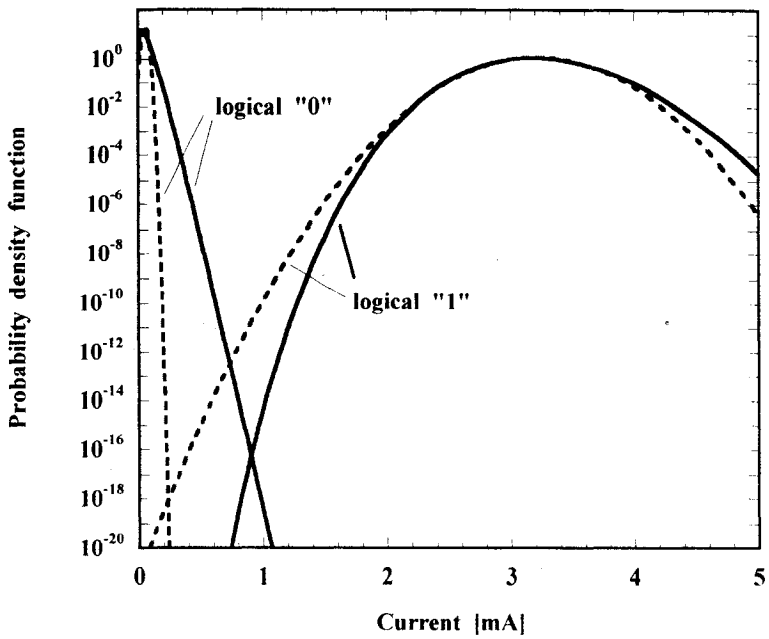

Fig. 4.10 The exact pdfs (solid) and Gaussian approximations (dashed) for DPSK receivers with single-port detection without the impact of nonlinear phase noise.

Fig.4.10 shows the exact pdfs (solid) and Gaussian approximations (dashed) for DPSK receivers with single-port detection without the impact of nonlinear phase noise. The parameters used in this calculation are the same as in Fig. 4.2. We find that the Gaussian approximation underestimates the bit error rate compared to the exact pdfs, and this will be discussed further below.

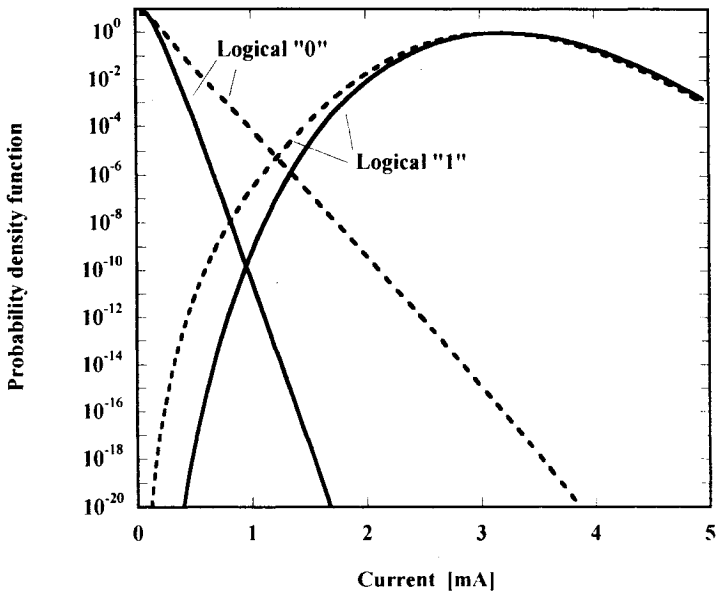

Fig.4.11 The exact pdfs for logical "1" and "0" in DPSK receiver with single-port detection without the impact of nonlinear phase noise (solid); and with the significant impact of nonlinear phase noise (dashed).

Fig.4.11 shows the exact pdfs with and without the impact of nonlinear phase noise in DPSK receiver with single-port detection. The parameters used in this calculation are the same as in Fig. 4.5. After comparing the inner tails of pdfs in Fig 4.11, we can make a conclusion that the performance of DPSK receiver with single-port detection may be degraded by the nonlinear phase noise.

We calculate the bit error rate by

$$BER = \frac{1}{2}\left[\int_{I_{th}}^{\infty} f_0(x)dx + \int_{-\infty}^{I_{th}} f_1(x)dx\right] \tag{4.57}$$

where $f_1(x)$ and $f_0(x)$ are the pdfs for bit "1" and "0" respectively. I_{th} is decision

current threshold.

Fig.4.12 shows BER for DPSK receivers with single-port detection and IM/DD receivers without the impact of nonlinear phase noise. The benefit of DPSK receivers vanishes when single-port detection is used, and the conventional Gaussian approximation underestimates the bit error rate, that agrees with the results in [42]. The parameters used in this calculation are the same as in Fig. 4.7.

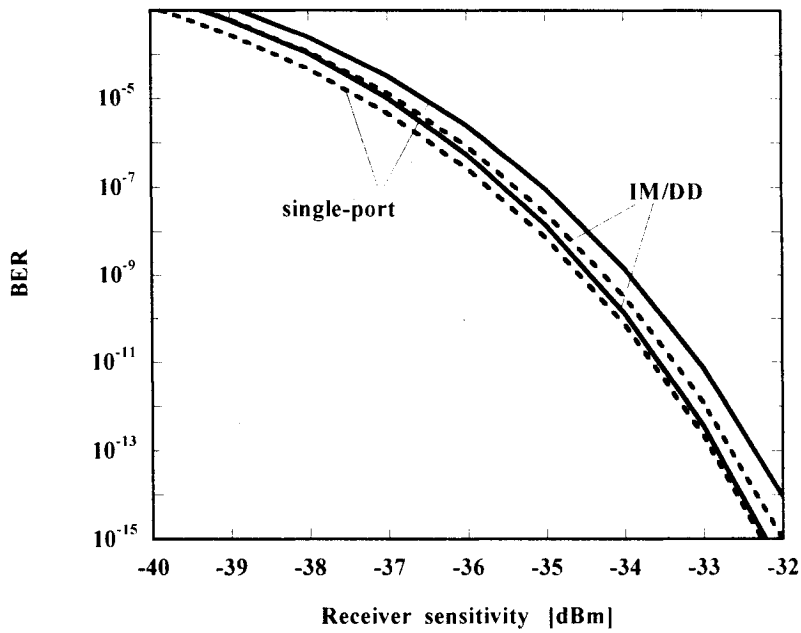

Fig.4.12 BER calculated by the exact pdf (solid) and Gaussian approximation (dashed) for DPSK receivers with single-port detection and IM/DD receivers without the impact of nonlinear phase noise.

Fig.4.13 shows BER with and without the impact of nonlinear phase noise in DPSK receivers with single-port detection. This further proves the performance of DPSK receiver with single-port detection may be degraded by the nonlinear phase noise. The

parameters used in this calculation are the same as in Fig. 4.8.

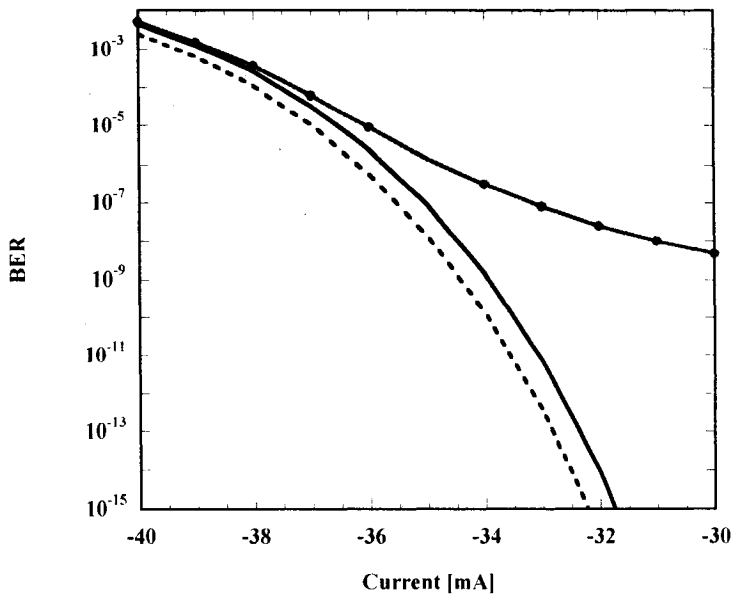

Fig.4.13 BER in DPSK receivers with single-port detection without the impact of nonlinear phase noise (solid), with the significant impact of nonlinear phase noise (solid and dots), and BER in IM/DD receivers (dashed).

4.4 Impact of Optical and Electrical Filters

In this section, we will discuss the influence of optical and electrical filters on the performance of ASE beat noise limited DPSK receivers.

The electrical noise power spectrum of beat noise has been studied in many books and papers. The signal-ASE and ASE-ASE beat noise power spectrums are illustrated in Fig. 4.14 and 4.15 for various locations in IM/DD receivers [7].

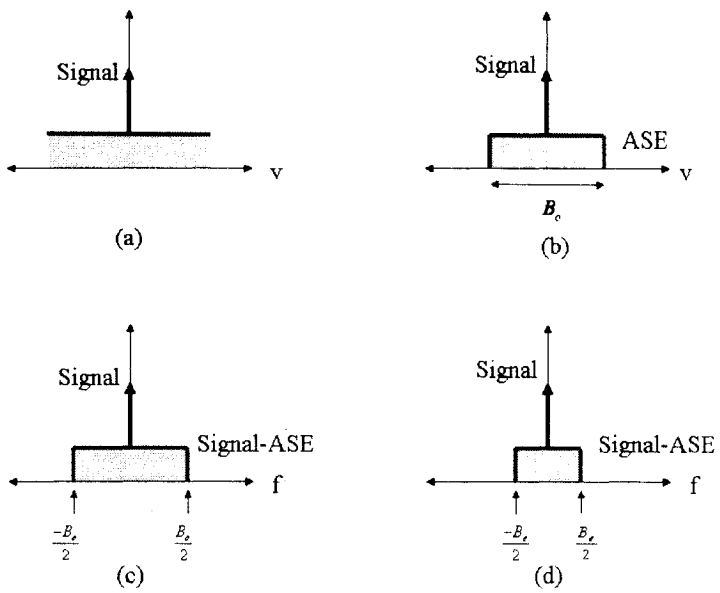

Fig. 4.14 The power spectrum of signal-ASE beat noise in the optically preamplified receiver, (a) after optical amplifier (b) after optical filter (c) after photodetector (d) after electrical filter.

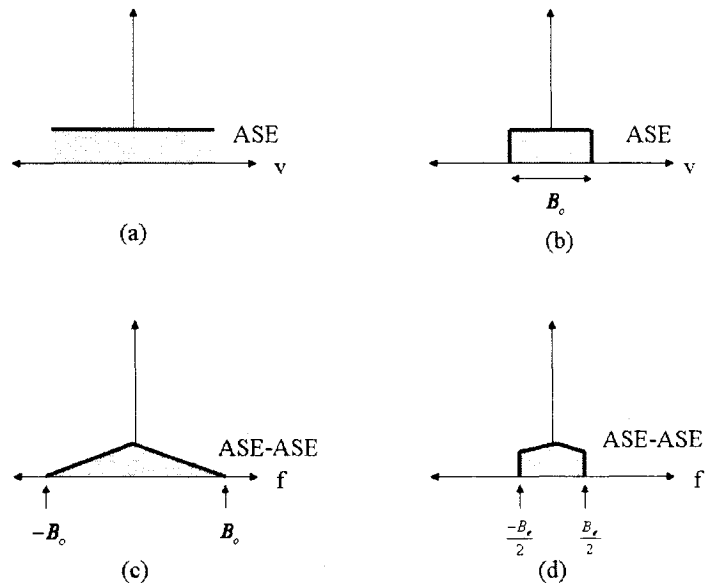

Fig.4.15 The power spectrum of ASE-ASE beat noise in the optically preamplified receiver, (a) after optical amplifier (b) after optical filter (c) after photodetector (d) after electrical filter.

For further studying the impacts of the optical and electrical filters, we calculate the

benefit of DPSK over IM/DD as a function of the ratio of optical over electrical filter bandwidth by using the exact pdfs. We assumed the electrical bandwidth B_e equals 0.7 times bit rate of 43 Gb/s, and we change the ratio of optical over electrical bandwidth from 1 to 5. From the Fig. 4.16, we can make a conclusion that the improvement of receiver sensitivity in DPSK systems over IM/DD is diminished at the high optical bandwidths, and this agree with the results in [32].

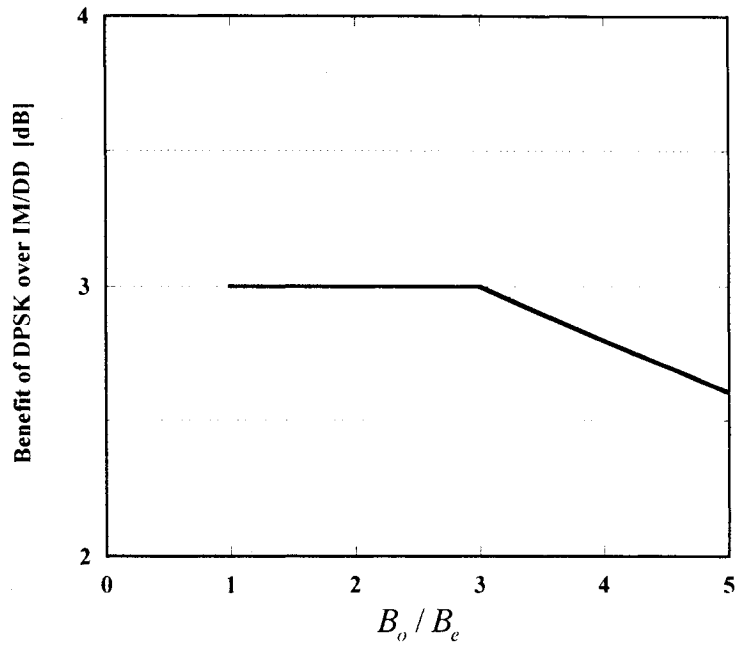

Fig. 4.16 The benefit of DPSK over IM/DD as a function of the ratio of optical and electrical filter bandwidth

Chapter 5

Conclusions

This thesis studied noise statistics in optically pre-amplified DPSK receivers with optical Mach-Zehnder interferometer demodulation. An exact mathematic model and Gaussian approximation have been given to analyze noise statistic of this receiver, and we compared the receiver performance by using theses two models. This chapter focuses on the summary of the above chapters and recommends for future research which are not included in this work.

5.1 Summary of Research

The introduction gave an overview of optical communications systems and some fundamental knowledge about optical modulation and detection technology.

Chapter 2 presented the structure of the DPSK system, and introduced the operation principle of components in this system.

Chapter 3 presented some fundamental knowledge and statistical properties of linearly additive noise and nonlinear phase noise.

Chapter 4 showed noise statistic analysis of the linearly additive noise and nonlinear phase noise, which are the dominant noise in the DPSK systems. Derivations of exact

analytical expressions and Gaussian approximations have been shown. We compared the difference of the noise statistic for DPSK and IM/DD receivers. The impact of optical and electrical filtering was also discussed in this Chapter.

5.2 Topics for Future Research

5.2.1 Inter-channel Cross-phase Modulation

In this thesis, we only considered the case of a single channel in the systems. In wavelength division multiplexed (WDM) systems, the nonlinear phase noise comes not only from the channel itself through self-phase modulation (SPM) but also from the other channels through cross-phase modulation (XPM) [9]. In the presence of XPM, pulses belonging to different WDM channels interact by shifting each other's phases.

In differential phase shift keying (DPSK) receivers, the signal-spontaneous emission beat noise introduces phase noise due to Kerr nonlinearity. In common 10-Gb/s dispersion-managed DWDM transmissions, the major nonlinear effects are self-phase modulation (SPM) and inter-channel cross-phase modulation (XPM) [43]. SPM is a single-channel effect, and XPM is a multi-channel effect: nonlinear phase noise is added to a given wavelength by converting the ASE-induced amplitude fluctuations in its adjacent WDM channels through inter-channel XPM. Since all the bits are having similar intensity profiles in DPSK, inter-channel XPM is much smaller in DPSK than in OOK.

5.2.2 RZ-DPSK

There are two choices for the modulation format of the resulting optical bit stream. These are shown in Fig. 5.1 and are known as the *return-to-zero* (RZ) and

nonreturn-to-zero (NRZ) formats. In the RZ format, each optical pulse representing bit "1" is shorter than the bit slot, and its amplitude returns to zero before the bit duration is over. In the NRZ format, the optical pulse remains on throughout the bit slot and its amplitude does not drop to zero between two or more successive "1" bits.

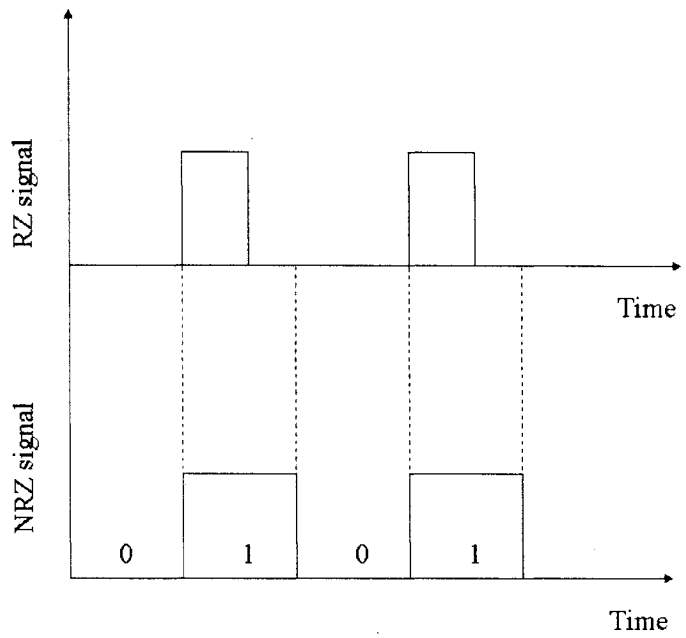

Fig. 5.1 NRZ and RZ formats

In practice, RZ formats typically have 1-3 dB better sensitivity than their NRZ equivalents and have more immunity to inter-symbol interference from transmitter and receiver impairments. A numerical simulation shows that RZ-DPSK has superior tolerance to nonlinear phase noise [35].

5.2.3 DQPSK

Differential quadrature phase shift keying (DQPSK) systems increase spectral efficiency and improve system tolerance to chromatic dispersion and polarization mode

dispersion (PMD). DQPSK format has 4 phase states: $\{0, \pi/2, \pi, 3\pi/2\}$. Two bits of information are included in each symbol, so bit rate is two times of symbol rate. The simulation results show a good performance of DQPSK system in term of chromatic dispersion and nonlinear effects tolerance in both single-channel and multiple-channel environments [44].

5.2.4 Dispersion

If we combine effects of ASE noise, Kerr nonlinearity, and chromatic dispersion on phase noise, the nonlinear phase noise will be modified by chromatic dispersion. Chromatic dispersion can either enhance or suppress the nonlinear noise amplification. For large absolute values of dispersion the nonlinear effect is suppressed, and the phase noise is reduced to its linear value. For a range of negative of dispersion, however, nonlinear phase noise is enhanced and exhibits a maximum related to the modulation instability found in amplitude fluctuations [25].

Reference

[1] R. Papannareddy, *Lightwave Communication Systems*, Arech House, 1997.

[2] G. P. Agrawal, *Fiber-Optic Communication Systems,* 3rd ed., John Wiley & Sons, Inc., New York, 2002.

[3] G. Keiser, *Optical Fiber Communications*, 3rd ed., McGraw-Hill, 2002.

[4] http://www.fiber-optics.info/fiber-history.htm

[5] D. Bailey and E. Wright, *Practical Fiber Optics*, Newnes, Burlington, 2003.

[6] I. T. Monroy and E. Tangdiongga, *Crosstalk in WDM Communication Networks*, Kluwer Academic Publishers, 2002.

[7] S. B. Alexnder, *Optical Communication Receiver Design*, SPIE Optical Engineering Press, 1997.

[8] T. Okoshi and K. Kikuchi, *Coherent Optical Fiber Communications*, KTK Academic Publishers, 1988.

[9] A.H. Gnauck et al., "2.3 Tb/s (64×42.7 Gb/s) transmission over 40×100km NZDSF using RZ_DPSK format and all-Raman-amplified spans", *OFC 2002,Postdeadline Paper FC2, pp. 17-22.*

[10] C. Rasmussen et al., "DWDM 40G transmission over trans-Pacific distance (10,000 km) using CSRZ_DPSK, enhanced FEC and all-Raman amplified 100km ultrawave fiber spans", *OFC 2003, PD 18.*

[11] J. Wang, and J. M. Kahn, "Impact of chromatic and polarization-mode dispersions

on DPSK systems using interferometric demodulation and direct detection", *J. Lightwave Technol., Vol.22, pp. 362-371, Feb. 2004.*

[12] C. Xu et al., "Comparison of return-to-zero differential phase-shift keying and on-off keying in long-haul dispersion managed transmission", *IEEE Photon Tech. Lett., Vol. 15, pp. 617-619, Apr. 2003.*

[13] X. Wei et al., "Optical $\pi/2$ -DPSK and its Tolerance to Filtering and Polarization-Mode Dispersion", *IEEE Photon. Tech. Lett., Vol. 15, pp. 1639-1641, Nov., 2003.*

[14] G. Bosco et al., "The effect of receiver imperfections on the performance of Direct-Detection optical systems using DPSK modulation", *OFC2003, vol. 2, pp. 457-458.*

[15] J. H. Sinsky et al., "RZ-DPSK transmission using a 42.7-Gb/s integrated balanced optical front end with record sensitivity", *J. of Lightwave Tech., Vol 22, pp. 180-185, Jan., 2004.*

[16] A. Hirano et al., "Performance of CSRZ-DPSK and RZ-DPSK in 43-Gbit/s/ch DWDM G.652 Single-Mode-Fiber transmission", *OFC 2003, Vol. 2, pp. 454-456.*

[17] P. J. Winzer and R. Essiambre, "Advanced optical modulation formats", *ECOC2003, Th 2.6.1.*

[18] A. H. Gnauck et al., "Demonstration of 42.7-Gb/s DPSK receiver with 45 photons/bit sensitivity", *IEEE Photon. Tech. Lett., Vol. 15, pp. 99-101, Jan., 2003* .

[19] M. T. Core and H. H. Tan, "BER for optical heterodyne DPSK receivers using delay demodulation and integration detection", *IEEE Transaction on Communications, Vol. 50, pp. 21-30, Jan., 2002.*

[20] C. Rasmussen et al., "DWDM 40G transmission over trans-pacific distance (10,000km) using CSRZ-DPSK, enhanced FEC and all-Raman amplified 100 km UltraWave fiber spans," *OFC2003 PD18.*

[21] P. J. Smith et al., "Optical heterodyne Binary-DPSK systems: A review of analysis and performance", *IEEE J. on Selected in Communications, Vol. 13, pp. 557-568, Apl. 1995.*

[22] P. J. Winzer and H. Kim, "Degradations in balanced DPSK receivers", *IEEE Photon. Tech. Lett., Vol. 15, pp. 1282-1284, Sep., 2003 .*

[23] D. Marcuse, "Derivation of analytical expressions for the bit-error probability in lightwave systems with optical amplifiers", *J. Lightwave Technol., Vol.8, pp. 1816-1823,1990.*

[24] D. Marcuse, "Calculation of bit-error probability for a lightwave system with optical amplifiers and post-detection Gaussian noise", *J. Lightwave Technol., Vol.9, pp. 505-513, Apr. 1991.*

[25] A. G. Green et al., "Effect of chromatic dispersion on nonlinear phase noise", *Optics Lett., Vol. 28, pp. 2455-2457, Dec. 2003.*

[26] H. Kim, A. H. Gnauck, "Experimental investigation of the performance limitation of DPSK systems due to nonlinear phase noise", *IEEE Photon. Tech. Lett., Vol.15, pp. 320-322, 2003.*

[27] P. J. Winzer and J. Leuthold, "Return-to-Zero modulation using a single NRZ drive signal and an optical delay interferometer", *IEEE Photon Tech. Lett., Vol. 13, pp. 1298 -1300, 2001.*

[28] H. Kolimbiris, *Fiber Optics Communications*, Pearson Prentice Hall, 2004.

[29] M. Bass and E. W. Van, *Fiber Optics Handbook*, McGraw-Hill, 2002.

[30] N. Grote and H. Venghaus, *Fibre Optic Communication Devices*, Springer. Berlin. 2001.

[31] S. V. Kartalopoulos, *DWDM Networks, Devices, and Technology*, John Wiley & Sons, Inc., New Jersey, 2003.

[32] P. J. Winzer et al., "Optimum filter bandwidths for optically preamplified NRZ receivers", *J. Lightwave Technol., Vol.19, pp. 1263-1273, Sep. 2001.*

[33] D. R. Goff, *Fiber Optic Reference Guide*, 3rd ed., Focal Press, 2002.

[34] E. Desurvire, *Erbium-Doped Fiber Amplifiers*, John Wiley & Sons, Inc., New Jersey, 2002.

[35] T. Mizuochi et al., "A comparative study of DPSK and OOK WDM transmission over transoceanic distances and their performance degradations due to nonlinear phase noise", *J. of Lightwave Tech., Vol 21, pp. 1933-1943, Sep., 2003.*

[36] O. Krauss, *DWDM and Optical Networks*, Publicis Corporate Publishing, Erlangen. 2002.

[37] J. P. Gordon and L. F. Mollenauer, "Phase noise in photonic communications systems using linear amplifiers", *Optics Lett., Vol. 15, pp. 1351-1353, Dec. 1990.*

[38] K.-P. Ho, "Asymptotic probability density of nonlinear phase noise," *Optics Letters, Vol.28, pp.1350-1352, 2003.*

[39] K.-P. Ho, "Probability density of nonlinear phase noise", *J. Opt. Soc. Am., Vol. 20, pp. 1875-1879, Sep. 2003.*

[40] A. Papoulis, and S. U. Pillai, *Probability, Random Variables and Stochastic Processes*, McGraw-Hill, 2002.

[41] Z. Qu, X. Zhang, and G. Yang, "Noise statistics in optically pre-amplified DPSK receivers with optical Mach-Zehnder interferometer demodulation", *Optics Letters, submitted for publication.*

[42] P. Winzer et al., "Impact of filtering on RZ-DPSK reception", *IEEE Photon Tech. Lett., Vol. 15, pp. 840 -842, 2003.*

[43] X. Liu, "Nonlinear effects in phase shift keyed transmission", *OFC2004, ThM4.*

[44] J. M. Gene et al., "Investigation of 10-Gb/s optical DQPSK systems in presence of chromatic dispersion, fiber nonlinearities, and phase noise", *IEEE Photon Tech. Lett., Vol. 16, pp. 924-926, Mar. 2004.*

Appendices

Appendix A: Derivation of Analytical Expressions for Linear Additive Noise [23, 24]

The amplified spontaneous emission noise has been expressed as a Fourier series that extends only over the interval T of one bit in this thesis. The signal pulse is represented in the same way. We present the optical signal in the time interval T of one bit by the complex representation $E_s(t) = E_1 \exp(i\omega_c t)$, ω_c is the angular carrier frequency. E_1 is the amplitude of optical carrier, and has been assumed a real constant. We represent the amplified spontaneous emission noise $e(t)$ as a Fourier series that is also defined only for the time duration T of one bit

$$e(t) = \sum_{v=0}^{\infty} c_v e^{i\omega_v t} \tag{A1}$$

with

$$\omega_v = \frac{2\pi}{T} v \tag{A2}$$

Note that the summation extends only over positive frequencies since we want $e(t)$ to correspond to the complex notation of the signal, the real part of these complex quantities represent the physical signal and noise. The expansion coefficients c_v of the noise are assumed to be independent Gaussian random variables with zero mean, and with a variance σ that is related to the noise power in the frequency band $1/T$ that is

occupied by one Fourier component.

Prior to entering the square-law detector, signal and noise are passed through an optical bandpass filter whose width is sufficient to permit the signal to pass unaltered. Its effect on the noise is to reject all frequencies outside of the passband of width B_o which extends from $v = v_1$ to $v = v_1 + M$ with

$$M = B_o T \tag{A3}$$

The filtered noise is simply represented by

$$e(t) = \sum_{v_1}^{v_1+M} c_v e^{j\omega_v t} \tag{A4}$$

The detector produces an electrical current that is proportional to the absolute square value of the sum signal and noise

$$I = K\left|E_s(t) + e(t)\right|^2 \tag{A5}$$

The current is averaged over the time duration of one bit so that the decision is based on the quantity

$$x = \frac{1}{T}\int_0^T I dt \tag{A6}$$

If there is only ASE-ASE beat noise occurs on the port, $E_s(t) = 0$. This leads to

$$x = K\sum_{v_1}^{v_1+M}(c_{rv}^2 + c_{iv}^2) \tag{A7}$$

where the absolute square magnitude of the complex expansion coefficients has been expressed as the sum of the squares of their real and imaginary parts. To reach our goal of deriving an expression for the probability density $f_0(x)$, we introduce its characteristic function

$$H_0(\zeta) = \int_0^\infty f_0(x) e^{i\zeta x} dx \tag{A8}$$

According to its definition, the characteristic function is defined as the average value of $\exp(i\zeta x)$. This average can be computed by introducing the probability densities for the real and imaginary parts of noise. Since all of them are independent Gaussian random variables, the characteristic function can be expressed as a 2-m fold integral over products of 2-M Gaussian probability densities. Substituting Eq. (A7) into this multiple integral and realizing that all integrals are actually identical, we obtain readily

$$H_0(\zeta) = \left\{ \frac{1}{\sqrt{2\pi}\sigma} \int_{-\infty}^{\infty} \exp\left[-\left(\frac{1}{2\sigma^2} - iK\zeta \right) u^2 \right] du \right\}^{2M} \tag{A9}$$

After performing the integration, we obtain

$$H_0(\zeta) = \frac{1}{(1 - 2iK\sigma^2\zeta)^M} \tag{A10}$$

The probability density is now obtained as the inverse of the Fourier integral Eq. (A10)

$$f_0(x) = \frac{1}{2\pi} \int_{-\infty}^{\infty} \frac{e^{-i\zeta x}}{(1 - 2iK\sigma^2\zeta)^M} d\zeta \tag{A11}$$

M integrations by parts convert this integral to the form

$$f_0(x) = \frac{1}{2\pi\Gamma(M)} \left(\frac{x}{2K\sigma^2} \right)^{M-1} \int_{-\infty}^{\infty} \frac{e^{-i\zeta x}}{1 - 2iK\sigma^2\zeta} d\zeta \tag{A12}$$

When $2iK\sigma\zeta = s$, we can write

$$f_0(x) = \frac{1}{2iK\sigma^2} \int_{-\infty}^{\infty} \frac{e^{-\frac{xs}{2K\sigma^2}}}{1 - s} ds \tag{A13}$$

By using the residue method

$$\int_{-\infty}^{\infty} R(x)dx = 2\pi i \sum_{k=1}^{n} \mathrm{Re}\, s[R(z), z_k] \tag{A14}$$

Eq. (A13) can be solved

$$f_0(x) = \left(\frac{M}{\overline{I}_n}\right)^M \frac{x^{M-1}}{\Gamma(M)} \exp\left[-M\frac{x}{\overline{I}_n}\right], x \geq 0 \tag{A15}$$

where $M = B_o / B_e$, the average current of ASE noise $\overline{I_n} = 2K\sigma^2 M$.

Next, we consider the combination effect of signal and noise, the current can be obtained by

$$I_1 = K[|E_1|^2 + E_s e^* + E_s^* e + |e|^2] \tag{A16}$$

Proceeding in close analogy to the procedure for computing $f_0(x)$, we obtain the following expression for the probability density $f_1(x)$

$$f_1(x) = \frac{1}{2\pi}\int_{-\infty}^{\infty} \frac{\exp\left[-\dfrac{2K\sigma^2 I_s \zeta^2}{1-2iK\sigma^2\zeta}\right]}{(1-2iK\sigma^2\zeta)^M} \exp[i(KI_s - x)\zeta]d\zeta \tag{A17}$$

This integral can be converted to a tabulated Laplace transform by using $1-2iK\sigma^2\zeta = S$, Eq. (A17) can be rewritten as

$$f_1(x) = \frac{e^{-\frac{I_s+x}{2k\sigma^2 M}}}{4i\pi k\sigma^2}\int_{-j\infty}^{+j\infty} \frac{1}{S^M} \exp\left(\frac{MI_s}{2K\sigma^2 MS} + \frac{MxS}{2K\sigma^2 M}\right) dS \tag{A18}$$

This is a tabulated Laplace transform, and it is solved as

$$f_1(x) = \frac{1}{2K\sigma^2}\left(\frac{x}{\overline{I}_s}\right)^{\frac{M-1}{2}} \exp\left(-M\frac{x+\overline{I}_1}{2K\sigma^2 M}\right) I_{M-1}\left(\frac{2\sqrt{x\overline{I}_s}}{2K\sigma^2}\right), x \geq 0 \tag{A19}$$

and it can be rewritten by using $\overline{I_n} = 2K\sigma^2 M$, Eq. (A19) can be rewritten as

$$f_1(x) = \frac{M}{\bar{I}_n}\left(\frac{x}{\bar{I}_1}\right)^{\frac{M-1}{2}} \exp\left(-M\frac{x+\bar{I}_1}{\bar{I}_n}\right) I_{M-1}\left(\frac{2M\sqrt{x\bar{I}_1}}{\bar{I}_n}\right), x \geq 0 \qquad \text{(A20)}$$

where $I_{M-1}(\ )$ is modified Bessel function, $\bar{I}_1$ is the average signal current, $\bar{I}_n$ is the average current of ASE noise, $M = B_o / B_e$, B_o is the optical noise bandwidth before the MZI, B_e is the electrical receiver bandwidth.

Appendix B: The Equivalent Noise Bandwidths of MZI

Supposed that the optical filter before the MZI is an ideal filter, i.e. $H_o(f)=1$ for $-B_o/2 < f < B_o/2$ and $H_o(f)=0$ elsewhere. The frequency responses of the ideal MZI are given by

$$H_{MZI}(f)=\begin{cases}\cos(\pi fT_b)\exp(-j\pi fT_b) & \text{cosntructive port}\\ \sin(\pi fT_b)\exp(-j\pi fT_b) & \text{destructive port}\end{cases} \quad \text{(B1)}$$

Thus, the equivalent noise bandwidths are given by

$$B_+ = \int_{-\infty}^{\infty}\left|H_{MZI}(f)\right|^2\left|H_o(f)\right|^2 df = \int_{-B_o/2}^{B_o/2}\cos^2(\pi fT_b)df = \frac{B_o}{2}+\frac{R_b}{2\pi}\sin(\pi B_oT_b) \quad \text{(B2)}$$

for the constructive port; and

$$B_- = \int_{-\infty}^{\infty}\left|H_{MZI}(f)\right|^2\left|H_o(f)\right|^2 df = \int_{-B_o/2}^{B_o/2}\sin^2(\pi fT_b)df = \frac{B_o}{2}-\frac{R_b}{2\pi}\sin(\pi B_oT_b) \quad \text{(B3)}$$

for the destructive port, where R_b is the bit rate.

Appendix C: Physical Constants and Conversions

c	velocity of light	$2.99792458\times10^{8} m/\sec$
e	electron charge	$1.60218\times10^{-19} Coulomb$
h	Plank's constant	$6.6260755\times10^{-34} J\cdot s$

$1rad = 360^{0} / 2\pi = 57.296^{0}$

$1eV = 1.60218\times10^{-19} Joule$

$$power(dBm) = 10\log_{10}[\frac{power(mW)}{1mW}]$$

Appendix D: Units in Decimal

10^N	Name
10^{15}	1 quadrillion
10^{12}	1 trillion
10^{9}	1 billion
10^{6}	1 million
10^{3}	1 thousand
10^{2}	1 hundred
10^{1}	Ten
10^{0}	One
10^{-1}	One-tenth
10^{-2}	One-hundred
10^{-3}	One-thousandth
10^{-6}	One-millionth
10^{-9}	One-billionth
10^{-12}	One-trillionth
10^{-15}	One-quadrillionth

Appendix E: Acronyms

ASE	amplified spontaneous emission
ASK	amplitude-shift keying
BER	bit-error rate
CW	continuous wave
DFB	distributed feedback
DPSK	differential phase-shift keying
DQPSK	differential quadrature phase-shift keying
EDFA	erbium-doped fiber amplifier
FP	Fabry-Perot
FSK	frequency-shift keying
FWHM	full-width at half-maximum
IM/DD	intensity modulation with direct detection
ISI	intersymbol interference
LAN	local-area network
LED	light-emitting diode
LO	local oscillator
LPF	low-pas filter
MAN	metropolitan-area network
NRZ	nonreturn to zero
OOK	on-off keying

PDF	probability density function
RZ	return to zero
SPM	self-phase modulation
WAN	wide-area network
WDM	wavelength-division multiplexing
XPM	cross-phase modulation